

# Jost function description of near threshold resonances for coupled-channel scattering

I. Simbotin, R. Côté\*

Department of Physics, University of Connecticut, 2152 Hillside Rd., Storrs, CT 06269, USA

## Abstract

We study the effect of resonances near the threshold of low energy ( $\varepsilon$ ) reactive scattering processes, and find an anomalous behavior of the  $s$ -wave cross sections. For reaction and inelastic processes, the cross section exhibits the energy dependence  $\sigma \sim \varepsilon^{-3/2}$  instead of the standard Wigner's law threshold behavior  $\sigma \sim \varepsilon^{-1/2}$ . Wigner's law is still valid as  $\varepsilon \rightarrow 0$ , but in a narrow range of energies. We illustrate these effects with two reactive systems, a low-reactive system ( $\text{H}_2 + \text{Cl}$ ) and a more reactive one ( $\text{H}_2 + \text{F}$ ). We provide analytical expressions, and explain this anomalous behavior using the properties of the Jost functions. We also discuss the implication of the reaction rate coefficients behaving as  $K \sim 1/T$  at low temperatures, instead of the expected constant rate of the Wigner regime in ultracold physics and chemistry.

**Keywords:** threshold resonances, ultracold chemistry, reactive scattering

## 1. Introduction

Ultracold gases allow a high level of control over the interaction by using Feshbach resonances [1] or by orienting ultracold molecules [2, 3]. In addition to the study of phenomena in degenerate quantum gases ranging from the BEC-BCS cross-over regime to solitons and multi-component condensates [4, 5], such control also permits the investigation of exotic three-body Efimov states [6]. In parallel, the rapid advances in forming cold molecules [7, 8, 9, 10, 11] have made possible studies of cold chemical reactions [2, 12] and their control [13], with application to a growing range of fields, such as quantum information processing [14, 15, 16]. A key ingredient for these investigations are resonances near the scattering threshold. Although such resonances have been theoretically [17] and experimentally [18, 19, 20] explored in the chemistry of low temperature systems, their effect on reaction rates is however not fully taken into account.

In this article, we investigate how reaction and inelastic processes are affected by near threshold resonances (NTR) in the entrance channel of a reactive scattering system. We focus our attention on two benchmark systems containing hydrogen, namely  $\text{H}_2 + \text{Cl}$  and  $\text{H}_2 + \text{F}$ . We note that alkali hydrides [21], because of their small mass, would also be interesting systems to investigate. By varying the mass of H, explore the modification of the behavior of the reaction cross section  $\sigma^{\text{react}}$  from the Wigner's threshold law  $\sigma^{\text{react}} \propto \varepsilon^{-1/2}$  [22, 23] at ultralow energy  $\varepsilon$ . We generalize our initial treatment [24] of the effect of resonances in low energy collisions originally analyzed in nuclear [25] and atomic [26] collisions, to include a multi-channel formalism using Jost functions.

In Section 2, we review the general theory of reactive scattering and discuss the two benchmark systems  $\text{H}_2 + \text{Cl}$  and  $\text{H}_2 + \text{F}$ , and present the results of our calculations in Section 3 for both systems. In Section 4, we give an explanation of those results based on the  $S$ -matrix, followed by an alternative description based on Jost functions in Section 5. Finally, we describe the equivalence of both approaches in Section 6 and give a simple physical picture in Section 7, before concluding in Section 8.

## 2. Reactive scattering at low energies

In this section, we review briefly the theory of low energy reactive scattering, and describe the two benchmark systems that we use to study the effect of  $s$ -wave near threshold resonances.

### 2.1. General theory

The scattering cross section from an initial internal state  $i$  to a final state  $f$  is given by [27]

$$\sigma_{f \leftarrow i}(\varepsilon_i) = \frac{\pi}{k_i^2} \sum_{J=0}^{\infty} \left( \frac{2J+1}{2j+1} \right) \sum_{\ell} \sum_{\ell'} |\delta_{fi} - S_{fi}^J|^2, \quad (1)$$

where  $\ell = |J - j|, \dots, J + j$  and  $\ell' = |J - j'|, \dots, J + j'$ ;  $\mathbf{J} = \mathbf{j} + \boldsymbol{\ell} = \mathbf{j}' + \boldsymbol{\ell}'$  is the total angular momentum, with molecular rotational momentum  $\mathbf{j}$  and orbital angular  $\boldsymbol{\ell}$  in the entrance channel  $i$ , and corresponding quantum numbers  $J$ ,  $j$ , and  $\ell$  (the primes indicate the exit channel  $f$ ). Here,  $\varepsilon_i = \hbar^2 k_i^2 / 2\mu$  is the kinetic energy with respect to the entrance channel threshold,  $k_i$  the wave number, and  $\mu^{-1} = m_{\text{H}_2}^{-1} + m_{\text{A}}^{-1}$  the reduced mass in the entrance arrangement (with A standing for Cl or F). We are focusing on the effect of resonances at ultralow temperatures, and so consider only  $s$ -wave scattering with  $\ell = 0$ , which requires  $J = j$  and thus  $(2J+1)/(2j+1) = 1$ . In addition, we limit

\*Corresponding author

Email address: rcote@phys.uconn.edu (R. Côté)

ourselves to molecules initially in their rotational ground state ( $j = 0$ ), such that we only need consider  $J = 0$ ; consequently, the sum  $\sum_{\ell'}$  in (1) reduces to a single term:  $\ell' = j'$ . Hence, equation (1) simplifies significantly, and it now reads:

$$\sigma_{f \leftarrow i}(\varepsilon_i) = \frac{\pi}{k_i^2} |\delta_{fi} - S_{fi}^{J=0}(k_i)|^2. \quad (2)$$

It is well known [28] that in the zero-energy limit the cross sections can be expressed in terms of the complex scattering length  $a_i = \alpha_i - i\beta_i$ ,

$$\begin{aligned} \sigma_i^{\text{react}}(\varepsilon) &\equiv \sum_{f \neq i} \sigma_{f \leftarrow i}(\varepsilon) \rightarrow 4\pi \frac{\beta_i}{k}, \\ \sigma_i^{\text{elast}}(\varepsilon) &\equiv \sigma_{i \leftarrow i}(\varepsilon) \rightarrow 4\pi(\alpha_i^2 + \beta_i^2). \end{aligned} \quad (3)$$

We obtain energy dependent rate coefficients by multiplying the cross sections with the relative velocity  $v_{\text{rel}} = \hbar k/\mu$ ,

$$\begin{aligned} K_i^{\text{react}}(\varepsilon) &\equiv \frac{\hbar k}{\mu} \sum_{f \neq i} \sigma_{f \leftarrow i}(\varepsilon) \rightarrow \frac{4\pi\hbar}{\mu} \beta_i, \\ K_i^{\text{elast}}(\varepsilon) &\equiv \frac{\hbar k}{\mu} \sigma_{i \leftarrow i}(\varepsilon) \rightarrow \frac{4\pi\hbar k}{\mu} (\alpha_i^2 + \beta_i^2), \end{aligned} \quad (4)$$

which can be thermally averaged over a Maxwellian velocity distribution to yield the true rate constant  $K(T)$ . Note that the sum  $\sum_{f \neq i}$  in Eqs. (3) and (4) includes all possible final states, i.e., both reaction channels to form the products and quenching (inelastic) channels for the reactant. Thus,  $\sigma^{\text{react}}$  and  $K^{\text{react}}$  defined above include all non-elastic outcomes of the scattering process, i.e., reaction plus quenching. We shall simplify our notation by omitting the channel subscript  $i$  (for  $\varepsilon_i$ ,  $k_i$ ,  $\alpha_i$ ,  $\beta_i$ , etc.) and we also omit the superscript  $J$  in  $S_{fi}^J$  throughout the remainder of this article.

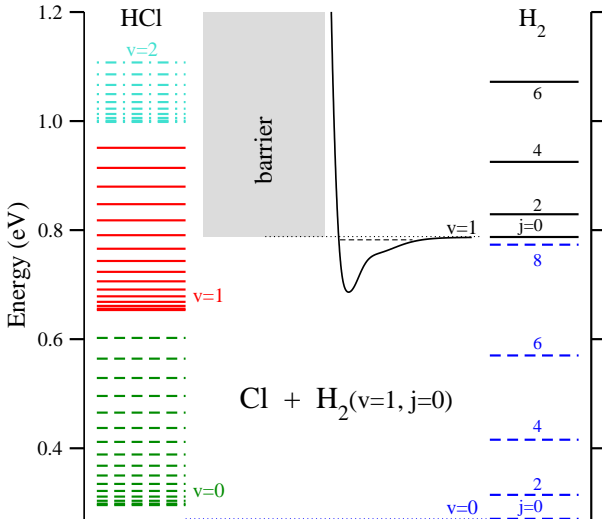


Figure 1: Rovibrational energy levels for  $\text{H}_2$  and  $\text{HCl}$ . For  $\text{H}_2$  we show the rotational series for  $v = 0$  (dashed blue) and  $v = 1$  (solid black). Similarly for  $\text{HCl}$ , we have  $v = 0$  (dashed green),  $v = 1$  (solid red) and  $v = 2$  (dot-dashed cyan). The inset shows a sketch of the diagonal matrix element of the potential energy surface for the ( $v = 1, j = 0$ ) ro-vibrational entrance channel; the dashed line represents a weakly quasi-bound level for the van der Waals complex  $\text{Cl} \cdots \text{H}_2$  in the entrance channel  $\text{H}_2(1,0)$ .

We remark that, although the limits in Eq. (3) remain valid even in the presence of NTRs, their applicability will be limited to a much narrower domain of energies, and a new behavior will emerge for the remainder of the low energy regime, as we will show in this article.

## 2.2. Systems with reaction barrier

For our study, we selected two barrier-dominated reactive systems, namely  $\text{H}_2 + \text{Cl} \rightarrow \text{H} + \text{HCl}$  and  $\text{H}_2 + \text{F} \rightarrow \text{H} + \text{HF}$ . Although both have reaction barriers, they have also different level structure energetics.

As shown in Fig. 1, low energy scattering is purely elastic for  $\text{Cl} + \text{H}_2$  with  $\text{H}_2$  in its rovibrational ground state. We therefore consider the next vibrational level as an initial state, namely ( $v = 1, j = 0$ ), such that the reaction to form  $\text{HCl}$  become possible even in the ultracold regime. Note that quenching of  $\text{H}_2$  by  $\text{Cl}$  will also be a possible (inelastic) outcome. Fig. 1 also shows the shallow potential well of the  $\text{Cl} \cdots \text{H}_2$  van der Waals complex which supports quasibound states leading to resonances in the entrance arrangement [29]. This system was recently investigated at ultralow temperatures by Balakrishnan [30] and by us [24]. In this work, we use the potential energy surface developed by Bian and Werner [31].

In the case of  $\text{H}_2 + \text{F}$ , reaction channels are already open, and the formation of  $\text{HF}$  at ultralow energies is possible even if  $\text{H}_2$  is in its rovibrational ground state ( $v = 0, j = 0$ ). Note that quenching is no longer possible in this case. However, there is a wide range of rovibrational states available for the product  $\text{HF}$ , as illustrated in Fig. 2. Again, the shallow potential well in the entrance channel can support quasibound states of the  $\text{F} \cdots \text{H}_2$  van der Waals complex, and if such a state is near the threshold, it will produce resonance effects for low energy scattering. This system has been studied in the ultracold regime by Dalgarno and co-workers [32, 33]. We use the potential energy surface developed by Stark and Werner [34].

As we did in our previous study of  $\text{H}_2 + \text{Cl}$  [24], we explore the effect of near threshold resonances (NTR) on reactive scattering by varying the mass of  $\text{H}$ . This was also done in [33]; the channel thresholds in both arrangements  $\text{H}_2\text{-Cl}$  and  $\text{H-HCl}$  (or  $\text{H}_2\text{-F}$  and  $\text{H-HF}$ ) shift at different rate, an approach similar to modifying the potential surface itself [35].

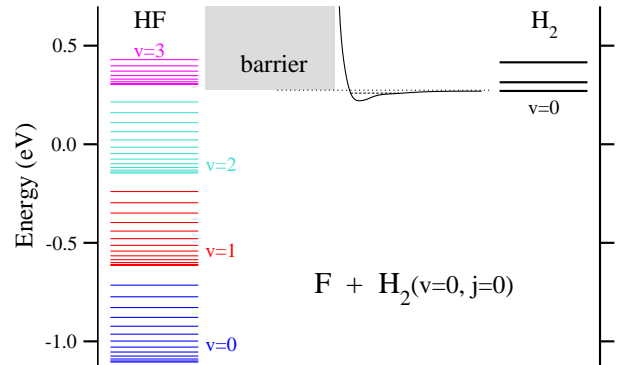


Figure 2: Same as Fig. 1 for  $\text{HF}$ . Only  $v = 0, j = 0, 2, 4$  are shown for  $\text{H}_2$ .

### 3. Results and discussion

The results we present here were obtained using the ABC reactive scattering code of Manolopoulos and coworkers [36], which we have optimized for ultralow energies in previous studies of  $\text{H}_2+\text{D}$  [37, 38, 39], and  $\text{H}_2+\text{Cl}$  [24].

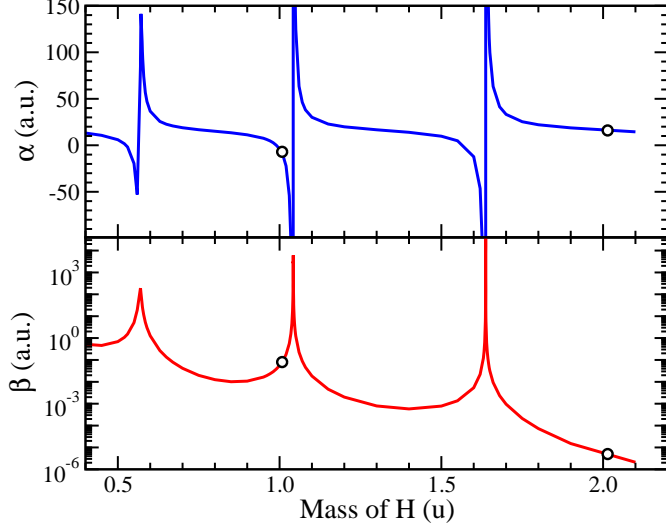


Figure 3: Real ( $\alpha$ ) and imaginary ( $\beta$ ) components of the scattering length as functions of the mass of the hydrogen atom  $m$  for  $\text{H}_2+\text{Cl}$ . The true masses of hydrogen and deuterium are indicated by circles.

#### 3.1. Results for $\text{H}_2 + \text{Cl} \rightarrow \text{HCl} + \text{H}$

Figure 3 shows the real and imaginary parts of the scattering length for  $\text{H}_2(v=1, j=0)+\text{Cl}$  as a function of the mass  $m$  of H, with the open circles indicating the true masses of H and D. We note that H is located on the wing of a resonance, visible as a sharp increase for  $\beta$ .

The top panel of Fig. 4 shows the reaction cross section as a function of  $m$  for a few energies (in Kelvin). The simple  $\sigma \propto k^{-1} \propto \varepsilon^{-1/2}$  scaling in Eq. (3) implies equidistant curves for the energies chosen in the logarithmic scale. We find this to be true except near the resonances. This is more clearly illustrated in the lower panel of Fig. 4 in which the rate constant is plotted; from Eq.(4), we expect curves to coincide for all those four low energies, which is the case away from the resonances. However, as we near a resonance, the difference between the curves become more pronounced.

In order to analyze this behavior, we selected three masses near the resonance, namely  $m = 1.0078 \text{ u} = m_{\text{H}}$  (true mass),  $1.038 \text{ u}$ , and  $1.042 \text{ u}$ ; they appear as dashed vertical lines in the inset of the top panel of Fig. 4. We focus our attention on these three masses, and we analyze in detail the energy dependence of the cross sections. Fig. 5(a) shows the low energy behavior of  $\sigma^{\text{react}}$ : as  $\varepsilon \rightarrow 0$ ,  $\sigma^{\text{react}}$  reaches the Wigner regime, scaling as  $\varepsilon^{-1/2}$  for all three masses, but for masses closer to the resonance, the scaling changes to  $\varepsilon^{-3/2}$ . Fig. 5(b) shows the elastic cross sections  $\sigma^{\text{elast}}$  for the same masses; the Wigner regime's constant cross section as  $\varepsilon \rightarrow 0$  changes to the expected  $\varepsilon^{-1}$  scaling for  $m$  near a resonance.

For the sake of completeness, the corresponding rate constants are plotted in Figs. 6(a) and (b). As  $m$  nears the resonance,  $K^{\text{react}}$  is significantly enhanced, scaling as  $T^{-1}$  until  $T$  is small enough that the Wigner regime is reached and  $K^{\text{react}}$  becomes constant. The corresponding scaling for  $K^{\text{elast}}$  changes from  $T^{-1/2}$  for NTR to  $T^{1/2}$  for Wigner's regime.

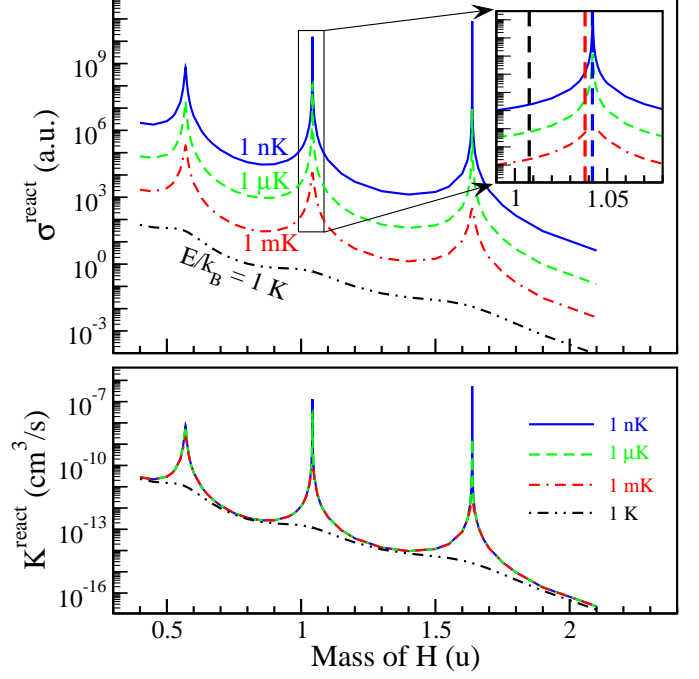


Figure 4: Top panel: Reaction cross section for  $\text{H}_2+\text{Cl}$  as a function of mass  $m$  of H for different scattering energies in units of Kelvin. The inset shows  $\sigma^{\text{react}}$  in the vicinity of the resonance with the vertical dashed lines corresponding to  $m = 1.0078 \text{ u} = m_{\text{H}}$  (true mass, in black),  $1.038 \text{ u}$  (red), and  $1.042 \text{ u}$  (blue), from left to right respectively. Bottom panel: Rate constant for the same energies.

#### 3.2. Results for $\text{H}_2 + \text{F} \rightarrow \text{HF} + \text{H}$

The results for the  $\text{F} + \text{H}_2(0,0)$  reaction contain resonant features that are similar to those described above for the  $\text{Cl} + \text{H}_2(1,0)$  system. Figure 7 shows the reaction rate constant at  $T = 0$ , which is directly related to  $\beta$ , see Eq. (4). Although Fig. 7 and Fig. 3 are similar, only two pronounced resonances are found for  $\text{H}_2 + \text{F}$ , even though the mass of H varies over a wider range. Note that the real mass of H is again on the wing of a resonance. Dalgarno and co-workers [33] have obtained similar results, but their work has explored a limited mass range (only up to  $m = 1.5 \text{ u}$ , with one additional data point for  $m = m_{\text{D}} \approx 2 \text{ u}$ ) and they only found one resonance (near  $m = 1.1 \text{ u}$ ).

The reaction cross section and rate constant follow the same behavior as the mass gets closer to the resonance. This is illustrated in Fig. 8 for  $\sigma^{\text{react}}$ , with the NTR scaling ( $\varepsilon^{-3/2}$ ) becoming more apparent as  $m$  gets closer to the resonance, while the Wigner regime (with  $\varepsilon^{-1/2}$  scaling) is pushed to lower energies. The corresponding behavior for the rate constant is shown in Fig. 9.

To explain the appearance of the NTR regime, we turn our attention to the analytical properties of the  $S$ -matrix.

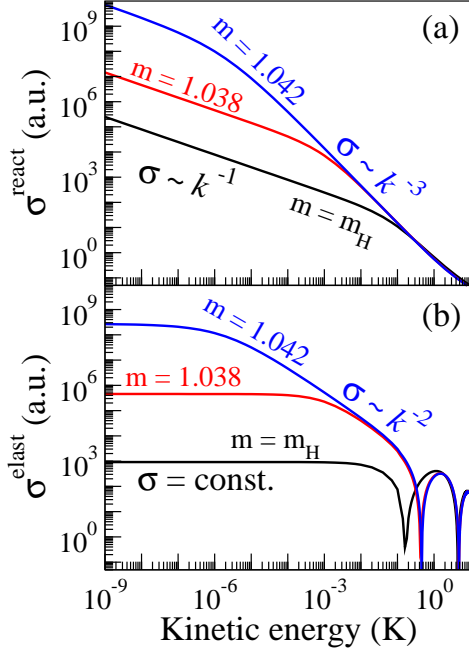


Figure 5: Energy dependence of the reaction cross section (a) and elastic cross section (b). The results shown are for the entrance channel  $\text{H}_2(v=1, j=0) + \text{Cl} \rightarrow \text{H} + \text{HCl}$ , and they correspond to different masses of H, as indicated for each curve.

#### 4. S-matrix approach for $\ell = 0$

The anomalous behavior of the cross sections shown above—an abrupt increase followed by a gradual transition into the Wigner regime, as the energy decreases—is due to the presence of a resonance pole near the threshold of the entrance channel. To understand this, we pay attention to the  $S$  matrix. Recalling the unitarity condition,  $\sum_f |S_{fi}|^2 = |S_{ii}|^2 + \sum_{f \neq i} |S_{fi}|^2 = 1$ , and using Eq. (2), we rewrite the cross sections in Eq. (3) explicitly in terms of the diagonal element  $S_{ii}(k)$ :

$$\sigma^{\text{react}}(k) = \frac{\pi}{k^2} (1 - |S_{ii}(k)|^2), \quad (5)$$

$$\sigma^{\text{elast}}(k) = \frac{\pi}{k^2} |1 - S_{ii}(k)|^2. \quad (6)$$

In this section we use the single channel case heuristically to guide our analysis of  $S_{ii}(k)$ , while in the next section we will present a more rigorous approach based on Jost matrices for the general case of a many channel problem.

##### 4.1. Pole factorization; single channel case

For a single channel problem, we express the  $S$  matrix for a given partial wave  $\ell$ , in terms of the Jost function  $\mathcal{F}_\ell$ :

$$S_\ell(k) = \frac{\mathcal{F}_\ell(-k)}{\mathcal{F}_\ell(k)}. \quad (7)$$

Thus, the properties of  $S_\ell(k)$  follow from those of the Jost function [40]; here, we shall make use of the fact that if  $\mathcal{F}_\ell(k)$  has a zero located at  $k = p$  (in the complex plane of the momentum), then the  $S$ -matrix has a pole at  $k = p$  and a zero at  $k = -p$ . Note that for any partial wave  $\ell \geq 1$ , two poles will approach

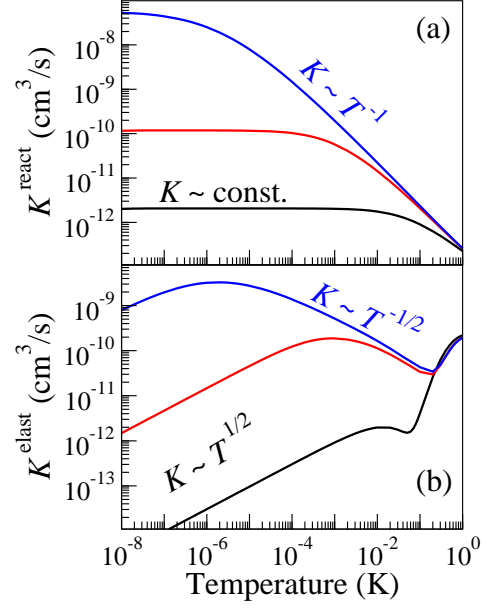


Figure 6: Temperature dependence of rate coefficients for reaction (a) and elastic scattering (b) corresponding to the cross sections shown in Fig. 5.

the threshold and collide at  $k = 0$ , while for s-wave ( $\ell = 0$ ) only a single pole at a time may reach the threshold. In this paper we analyze the case of s-wave scattering, for which it is convenient to factor out the effect of the pole at  $k = p$  and its accompanying zero at  $k = -p$ . Thus, we can write

$$S(k) = \frac{p+k}{p-k} \tilde{S}(k), \quad (8)$$

and we assume the background contribution  $\tilde{S}(k)$  is a slowly varying function of  $k$ . Note that we shall omit the subscript  $\ell$ , as we only discuss the case of  $\ell = 0$ .

As is well known [40], for purely elastic scattering in partial wave  $\ell = 0$ , a pole  $p$  which is sufficiently close to  $k = 0$  will be located on the imaginary axis; thus, we can write

$$p = i\kappa, \quad (9)$$

with  $\kappa$  real valued; when  $\kappa > 0$  the pole corresponds to a bound state, while for  $\kappa < 0$  it corresponds to a virtual (or anti-bound) state. Since we are interested in near threshold resonances, we shall focus our attention on a short segment of the trajectory of the pole along the imaginary axis near  $k = 0$ . From Eqs. (9) and (8) it is clear that the resonant contribution  $S^{\text{res}}(k) \equiv \frac{p+k}{p-k} = \frac{i\kappa+k}{i\kappa-k}$  is explicitly unitary for real values of  $k$ . The full  $S$  matrix is also unitary for real  $k$ , and thus the background part has to be unitary, and both of them can be written in the usual fashion, i.e.,  $S = e^{2i\delta}$  and  $\tilde{S} = e^{2i\tilde{\delta}}$ . The full phaseshift  $\delta$  is a sum of the background phaseshift  $\tilde{\delta}$  and the resonant contribution,

$$\delta(k) = \tilde{\delta}(k) - \arctan\left(\frac{k}{\kappa}\right).$$

Hence, the elastic cross section,  $\sigma^{\text{elast}} = \frac{4\pi}{k^2} \sin^2 \delta$ , reads

$$\sigma^{\text{elast}}(k) = \frac{4\pi}{k^2} \frac{(k \cos \tilde{\delta} - \kappa \sin \tilde{\delta})^2}{k^2 + \kappa^2}.$$



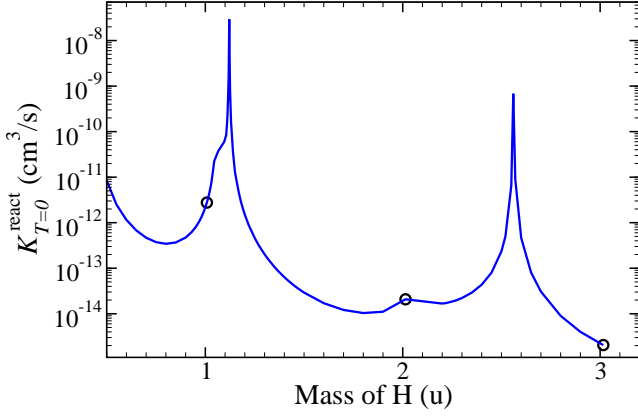


Figure 7: Mass dependence of the reaction rate coefficient for  $F + H_2(0,0) \rightarrow HF + H$  at  $T = 10^{-6}K$ .

At low energy we use the approximation  $\sin \tilde{\delta} \approx \tilde{\delta}(k) \approx -k\tilde{a}$  (and  $\cos \tilde{\delta} \approx 1$ ) to further simplify the expression above:

$$\sigma^{\text{elast}}(k) \approx 4\pi \frac{(1 + \kappa\tilde{a})^2}{k^2 + \kappa^2} = 4\pi a^2 \frac{\kappa^2}{k^2 + \kappa^2}, \quad (10)$$

where  $\tilde{a}$  is the background scattering length, and  $a = \tilde{a} + \frac{1}{\kappa}$  the full scattering length. We remark that the Lorentzian expression in the equation above is a function of the *momentum*  $k$ . Thus, although Eq. (10) is similar to the Breit–Wigner formula, we recall that the latter has the familiar Lorentz-type *energy* dependence. Moreover, since the lineshape in Eq. (10) is centered on the threshold ( $k = 0$ ) itself, only the  $k > 0$  half can be probed in elastic scattering, which is specific to the case of a near threshold resonance for partial wave  $\ell = 0$  in the entrance channel.

When the resonant pole crosses the threshold, the scattering length diverges:

$$a = \tilde{a} + \kappa^{-1} \xrightarrow{\kappa \rightarrow \pm 0} \pm\infty. \quad (11)$$

Hence, the behavior of the cross section will be affected dramatically; indeed, when  $\kappa$  is vanishingly small, the denominator in Eq. (10) will give rise to two different types of behavior inside the low energy domain, depending on the relative magnitude of  $\kappa$  and  $k$ . When  $k \ll |\kappa|$  we recover the familiar result for the Wigner regime,

$$\sigma^{\text{elast}}(k) \xrightarrow{k \rightarrow 0} 4\pi a^2,$$

while for the remainder of the low energy domain,  $\kappa$  becomes negligible when  $k \gg |\kappa|$ , and we obtain

$$\sigma^{\text{elast}}(k) \xrightarrow{k \gg |\kappa|} 4\pi \frac{(1 + \kappa\tilde{a})^2}{k^2} \xrightarrow{\kappa \approx 0} \frac{4\pi}{k^2},$$

which we refer to as *NTR-regime behavior*. From our discussion, it is clear that the extent of the NTR regime is specified approximately by the inequalities  $|\kappa| \lesssim k \lesssim |\tilde{a}|^{-1}$ .

We emphasize that although the Wigner regime can be displaced towards the extreme low energy domain, Wigner’s threshold law is always recovered when  $k \rightarrow 0$ , except in the critical

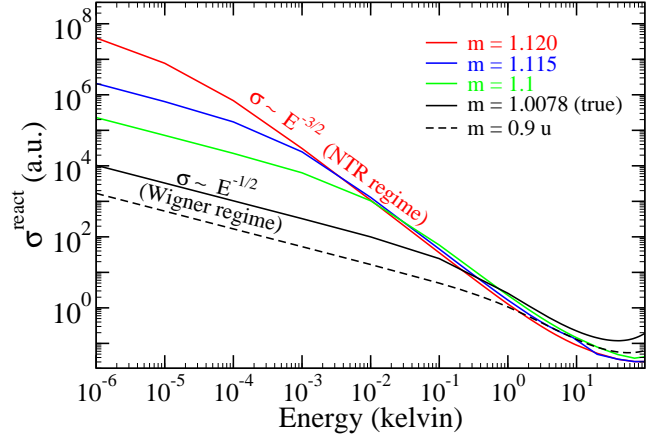


Figure 8: Energy dependence of the reaction cross section for  $F + H_2(0,0)$  for different masses of H.

case of  $\kappa = 0$ , which corresponds to a bona fide zero-energy resonance. Only in this special case, could the Wigner behavior be lost, and  $\sigma^{\text{elast}}(k)$  would diverge at  $k = 0$ , since it would follow the NTR-regime behavior throughout the entire low- $k$  regime. As we shall see in the next section, the special case of a zero-energy resonance is only possible for purely elastic scattering, because any additional (inelastic or reactive) open channels—which are coupled, however feebly, to the entrance channel—will push the resonance pole away from the imaginary axis; hence, the pole will be kept away from  $k = 0$ , but still possibly close enough to produce a significant resonance effect.

#### 4.2. Pole factorization; many channel case

We consider first the reaction cross section, followed by the elastic cross section.

##### 4.2.1. The reaction cross section

We now extend the analysis of the single channel  $S$  matrix to the many channel case; namely, we focus on the diagonal element  $S_{ii}(k)$  corresponding to the entrance channel. It is important to note that the factorization employed in the single channel

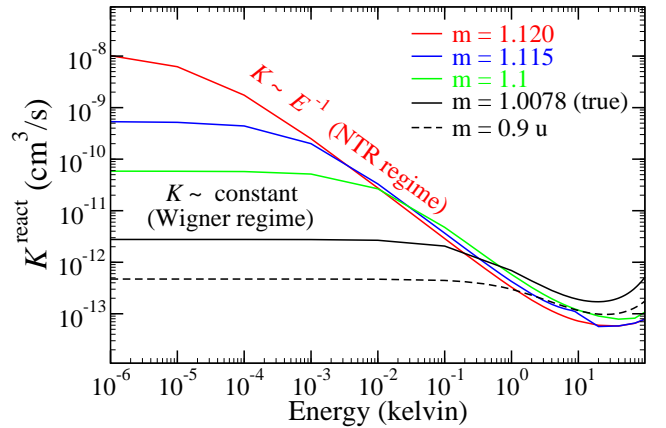


Figure 9: Energy dependence of the reaction rate constant for  $F + H_2(0,0)$  for different masses of H.

case in Eq. (8) also holds for the diagonal element corresponding to the entrance channel; indeed, the general properties of the  $S$  matrix ensure that a pole at  $k = p$  is always accompanied by a zero of  $S_{ii}(k)$  at  $k = -p$  [41]. Thus, for a NTR in the entrance channel  $i$ , we write

$$S_{ii}(k) = \frac{p+k}{p-k} \tilde{S}_{ii}(k). \quad (12)$$

The background contribution  $\tilde{S}_{ii}(k) = e^{2i\tilde{\delta}_i}$  is again assumed to be a slowly varying function of  $k$ . However, unlike the single-channel case, the background phase shift  $\tilde{\delta}_i$  is now a complex quantity (owing to the nonzero reactivity of the system). Moreover, the pole  $p$  is no longer on the imaginary axis, as will be illustrated by our results, and can be explained by the fact that a quasi-bound state of the van der Waals complex near the threshold of the entrance channel can decay in all available (open) channels, and thus has a finite lifetime and a finite decay rate. Should the pole be located on the imaginary axis in the momentum plane, it would then be located on the real energy axis in the energy plane, implying a zero width (decay rate  $\Gamma = 0$ ) and thus an infinite lifetime of complex, which would contradict the assumption of nonzero reactivity.

Our results will show that  $\text{Re}(p)$  is always negative; thus, we write explicitly:

$$p = -q + ik,$$

with  $q > 0$ . The nonzero value of  $q$  stems from the nonzero reactivity (inelasticity) of the system, as argued above. Hence, the eigen-energy  $E_p = p^2/2\mu$  associated with the pole is now a complex quantity, with  $\text{Re}(E_p) = (q^2 - \kappa^2)/2\mu$  and  $\text{Im}(E_p) = -q\kappa/\mu$ . The algebraic sign of  $\kappa$  will determine if the pole represents a virtual state or a quasi-bound state of the van der Waals complex; indeed, just as in the single channel case,  $\kappa > 0$  corresponds to the latter, while  $\kappa < 0$  to the former. We remark that the decay rate  $\Gamma = -2\text{Im}(E_p) = 2q\kappa/\mu$  is positive for a quasi-bound van der Waals complex, while for a virtual state we have  $\Gamma < 0$  (unphysical).

At low energy, we employ the usual parametrization of the background contribution,  $\tilde{\delta}_i(k) \approx -k\tilde{a}_i$ , where the background scattering length  $\tilde{a}_i = \tilde{\alpha}_i - i\tilde{\beta}_i$  is now a complex quantity. Using similar parametrizations, the resonant part and the full  $S$  matrix element in Eq. (12) can be linearized when  $k \rightarrow 0$ . Thus we have  $S_{ii}^{\text{res}}(k) = \frac{p+k}{p-k} \approx 1 - 2ia_i^{\text{res}}k$ , and  $S_{ii}(k) = S_{ii}^{\text{res}}(k)\tilde{S}_{ii}(k) \approx 1 - 2ia_ik$ , and we can extract the resonant contribution to the scattering length,  $a_i^{\text{res}} = \frac{i}{p} = \frac{\kappa - iq}{q^2 + \kappa^2}$ , and the full scattering length  $a_i = \tilde{a}_i + a_i^{\text{res}} = \tilde{a}_i + \frac{i}{p}$ . Omitting the channel subscript, the real and imaginary parts of the scattering length read:

$$\text{Re}(a) \equiv \alpha = \tilde{\alpha} + \frac{\kappa}{q^2 + \kappa^2}, \quad (13)$$

$$-\text{Im}(a) \equiv \beta = \tilde{\beta} + \frac{q}{q^2 + \kappa^2}. \quad (14)$$

We now return to the *unapproximated* expression of the resonant contribution in Eq. (12),  $S^{\text{res}}(k) = \frac{p+k}{p-k}$ , and the full  $S$  matrix element,  $S(k) = \frac{p+k}{p-k} e^{-2ik\tilde{a}}$ , which are valid for the entire low-energy domain, namely  $k \lesssim |\tilde{a}|$ . Making use of

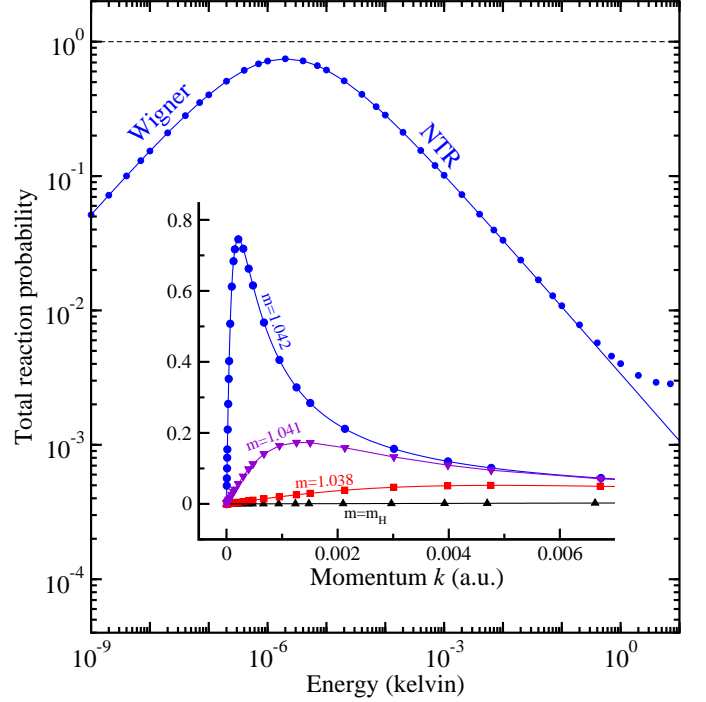


Figure 10: Low energy behavior of the total reaction probability for  $m = 1.042$  u in  $\text{H}_2 + \text{Cl}$ . The horizontal dashed line marks the unitarity limit. Inset: linear-scale plot of  $P^{\text{react}}(k)$  for different masses (as indicated). The data points from the full (exact) computation are shown as symbols, while the continuous lines were obtained by fitting using Eq. (20).

$|\tilde{S}(k)|^2 \approx |e^{-2ik\tilde{a}}|^2 = e^{-4k\tilde{\beta}}$ , and substituting Eq. (12) in Eq. (5), the reaction cross section reads:

$$\sigma^{\text{react}} = \frac{\pi}{k^2} \frac{2e^{-2k\tilde{\beta}}}{|p-k|^2} \left[ (k^2 + |p|^2) \sinh 2k\tilde{\beta} + 2qk \cosh 2k\tilde{\beta} \right], \quad (15)$$

Assuming low reactivity, i.e.,  $\tilde{\beta} \rightarrow 0$ , this result can be further simplified:

$$\sigma^{\text{react}}(k) \approx 4\pi \frac{\beta}{k} \left| \frac{p}{p-k} \right|^2, \quad (16)$$

with  $\beta$  given in Eq. (14). Finally, if one neglects  $\tilde{\beta}$  entirely, one can substitute  $\beta \approx \beta^{\text{res}} = q|p|^{-2}$  in the equation above, which can be recast as

$$\sigma^{\text{react}}(k) \approx \frac{4\pi}{k} \frac{q}{(q+k)^2 + \kappa^2}. \quad (17)$$

This expression only contains two parameters ( $q$  and  $\kappa$ ) which are sufficient to describe a prominent NTR (when  $\tilde{\beta}$  is small). Note that the full expression given in Eq. (15) includes the background contribution  $\tilde{\beta}$  as a third parameter, which allows for slight deviations from the simple  $k$ -dependence in Eq. (17).

Recall that we are interested in the case when  $|p|$  is very small, such that the energy associated with the pole,  $|E_p| = \frac{1}{2\mu} \hbar^2 |p|^2$ , is well within the ultracold domain. Consequently, there will be two different types of behavior at low  $k$ , depending on the relative values of  $k$  and  $|p|$ . Indeed, for  $k \ll |p|$ , we recover Wigner's threshold law,

$$\sigma^{\text{react}} \xrightarrow[k \rightarrow 0]{} 4\pi \frac{\beta}{k}, \quad (18)$$

while for  $k \gg |p|$ , Eq. (17) reduces to

$$\sigma^{\text{react}} \xrightarrow{k \gg |p|} 4\pi \frac{q}{k^3}, \quad (19)$$

which we named NTR-regime behavior.

We emphasize that the simple expression in Eq. (17) captures both types of behavior, including the transition between the two regimes, and we can employ it to fit our computed data. Specifically, we use a more convenient quantity than the cross section shown in Fig. 5(a), namely the reaction probability,  $P^{\text{react}} \equiv 1 - |S_{ii}|^2 = \frac{k^2}{\pi} \sigma^{\text{react}}(k)$ , which is bound between zero and one. Hence, our fitting procedure employs the expression

$$P^{\text{react}}(k) = 4q \frac{k}{(q+k)^2 + \kappa^2}, \quad (20)$$

which is equivalent with Eq. (17). The asymmetrical profile of  $P^{\text{react}}(k)$  is clearly illustrated by the linear-scale plot shown as an inset in Fig. 10, which contains results for various masses, ranging from the true mass of hydrogen ( $m = m_{\text{H}}$ ) to  $m = 1.042$  u. The results for one of the strongly resonant cases ( $m = 1.042$  u) are also shown on a log-log scale (see the main plot in Fig. 10), which emphasizes the good agreement between the numerical results and the simple analytical expression in Eq. (20). Also, the two power-laws in Eqs. (18) and (19) are easily recognized on the log-log plot in Fig. 10; indeed, we have  $P^{\text{react}}(k) \sim k$  in the Wigner regime, and  $P^{\text{react}}(k) \sim k^{-1}$  in the NTR regime.

From Eq. (20) it follows that  $P^{\text{react}}(k)$  reaches its maximum value at  $k_{\text{max}} = |p|$ , which marks the transition between the two regimes; in terms of energy, the maximum of  $P^{\text{react}}$  is located at  $E_{\text{max}} = |E_p| = \frac{1}{2\mu}(q^2 + \kappa^2)$ . Although it is tempting to interpret the location of the maximum of  $P^{\text{react}}(k)$  as the position of the resonance, one has to resist this temptation. Indeed, based on Eq. (20), we suggest that it is more appropriate to assign  $k = -q$  as the position of the resonance, instead of  $k = k_{\text{max}} = |p|$ .

We remark that the unitarity limit ( $P^{\text{react}} = 1$ ) can only be reached in the special case with  $\kappa = 0$ , when the pole is situated on the negative real axis at  $p = -q$ , and the diagonal element of  $S$  corresponding to the entrance channel has a zero on the positive real axis at  $k = -p = q$ . Namely, we have  $S_{ii}(q) = 0$ , see Eq. (12), which guarantees that  $P^{\text{react}}(q) = 1$ . Figure 11 shows the pole trajectory in the complex plane as a function of the parameter  $m$ , and makes it apparent that the trajectory  $p(m)$  crosses the real axis when  $m$  reaches a critical (resonant) value  $m = m_{\text{res}}$ . We note that in the special case of  $m = m_{\text{res}}$ , when the unitarity limit  $P^{\text{react}}(k) = 1$  is reached at  $k = q(m_{\text{res}})$ , the NTR regime extends to the lowest possible energies into the ultracold regime:  $k \lesssim |p(m_{\text{res}})| = q(m_{\text{res}})$ . When  $m$  moves gradually away from  $m_{\text{res}}$  the NTR regime shrinks gradually, and it spans a narrower range of energies (as seen in Figs. 5, 6, 8, and 9). Eventually, the NTR regime disappears when the pole  $p(m)$  is no longer in the vicinity of  $k = 0$ .

The pole parameters  $q = -\text{Re}(p)$  and  $\kappa = \text{Im}(p)$  are treated as fitting variables, and they are thus obtained from the computed results. Note that the value of  $\tilde{\beta}$  can only be extracted from the fitting procedure if the full expression in Eq. (15) is employed instead of the simpler Eq. (17); we also remark that

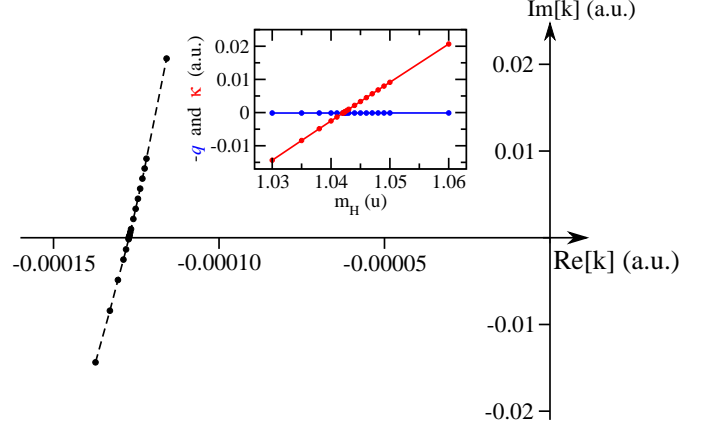


Figure 11: Pole trajectory in the complex plane of the momentum for  $\text{H}_2 + \text{Cl}$ . The inset shows the explicit mass dependence of  $q = -\text{Re}[p]$  and  $\kappa = \text{Im}[p]$ . Note that  $q(m)$  is nearly constant, while  $\kappa(m)$  has an almost linear behavior. Also note that  $|\kappa|$  increases considerably on either side of the resonance, such that  $q \ll |\kappa|$  (except near the very center of the resonance, where  $\kappa \approx 0$ ).

when  $\tilde{\beta}$  is negligibly small compared to the resonant contribution  $\beta^{\text{res}} = q(q^2 + \kappa^2)^{-1}$ , see Eq. (14), then it can no longer be extracted reliably from the fitted data.

We emphasize that we conducted our analysis in the complex plane of the momentum  $k$ , rather than the complex energy plane; to appreciate the unsuitability of the latter, we simply point out that the complex energies associated with both the pole ( $k = p$ ) and the zero ( $k = -p$ ) are identical,

$$E_p = \frac{\hbar^2(\pm p)^2}{2\mu} \equiv \varepsilon_p - i\hbar \frac{\Gamma}{2}, \quad (21)$$

with  $\varepsilon_p = \frac{\hbar^2}{2\mu}(q^2 - \kappa^2)$  and  $\Gamma = \frac{2\hbar}{\mu}q\kappa$ . We recall that one must have  $q > 0$  for a physical cross section, see Eq. (17), and thus we have  $\text{sgn}(\Gamma) = \text{sgn}(\kappa)$ . Hence, for a quasi-bound vdW-complex ( $\kappa > 0$ ) we have  $\Gamma > 0$ , while for the case of a virtual state ( $\kappa < 0$ ) we have  $\Gamma < 0$  (unphysical). Finally, we remark that for an  $s$ -wave NTR, scattering alone cannot distinguish between shallow bound and anti-bound (virtual) states, because  $\sigma^{\text{react}}(k)$  does not depend on  $\text{sgn}(\kappa)$ , see Eq. (15).

#### 4.2.2. The elastic cross section

For the sake of completeness, we also give the expression of the elastic cross section. Employing again the parametrization  $\tilde{S} = e^{-2i\tilde{\alpha}k}e^{-2\tilde{\beta}k}$  in Eq. (12), which is then substituted in Eq. (6), we obtain

$$\sigma^{\text{elast}} = \frac{\pi}{k^2} \frac{2e^{-2k\tilde{\beta}}}{|p-k|^2} \left[ (k^2 + |p|^2) \cosh 2k\tilde{\beta} + 2k\kappa \sin 2k\tilde{\alpha} + (k^2 - |p|^2) \cos 2k\tilde{\alpha} + 2kq \sinh 2k\tilde{\beta} \right].$$

Under the assumption of low reactivity,  $\tilde{\beta} \rightarrow 0$ , which is a requirement for having pronounced NTRs, we obtain

$$\sigma^{\text{elast}} = 4\pi|a|^2 \left| \frac{p}{p-k} \right|^2,$$

where  $a = \alpha - i\beta$  is the full scattering length. Although the expressions for the elastic cross section given above contain four

parameters ( $\tilde{\alpha}$ ,  $\tilde{\beta}$ ,  $q$  and  $\kappa$ ), only two of them are needed when the resonance pole is very close to the threshold ( $p \approx 0$ ). Indeed, if the pole contribution is dominant, we can neglect  $\tilde{a}$ , and use  $a \approx a^{\text{res}} = \frac{i}{p}$  in the equation above, which we rewrite as

$$\sigma^{\text{elast}} = \frac{4\pi}{(q+k)^2 + \kappa^2}. \quad (22)$$

Note the similarity between this result for the elastic cross section and Eq. (17) for the reactive cross section; thus, in the limit  $k \rightarrow 0$  we recover again the familiar Wigner behavior,

$$\sigma^{\text{elast}} \xrightarrow{k \rightarrow 0} 4\pi|a|^2,$$

and for the NTR regime we obtain

$$\sigma^{\text{elast}} \xrightarrow{k \gg |p|} \frac{4\pi}{k^2}.$$

## 5. Jost-function approach

We now describe an alternative approach, based on the use of the Jost function, to obtain the anomalous  $k^{-3}$  scaling of the reaction cross section for the NTR regime described in the previous section. We shall first give the key concepts for the case of single channel and short-range interaction  $V(R)$ , and generalize the results to the multi-channel case afterward.

### 5.1. Single channel case

The regular solution of the radial equation,

$$\frac{d^2}{dR^2}\phi_k = [2\mu V(R) - k^2]\phi_k(R),$$

is uniquely specified by initial-value type conditions:  $\phi_k = 0$  and  $\frac{d}{dR}\phi_k = 1$  at  $R = 0$ . Recall that we are discussing only the case of s-wave ( $\ell = 0$ ) scattering; for higher partial waves, the initial boundary condition reads:  $\phi_{k,\ell}(R) \sim R^{\ell+1}$ . The asymptotic behavior of the regular solution can be written as

$$\phi_k(R) \xrightarrow{R \rightarrow \infty} \frac{1}{k}[A(k) \sin kR + B(k) \cos kR]. \quad (23)$$

If  $k$  is real valued, and assuming  $V(R)$  is real, then we can choose  $\phi_k$  to be real; hence,  $A(k)$  and  $B(k)$  are real valued. Recasting Eq. (23) in terms of the free solutions  $\exp(\pm ikR)$ , we have

$$\phi_k(R) \xrightarrow{R \rightarrow \infty} \frac{i}{2k}[(A - iB)e^{-ikR} - (A + iB)e^{+ikR}], \quad (24)$$

and following the convention used in Refs. [40, 42], we define the Jost function:

$$\mathcal{F}(k) \equiv A(k) - iB(k). \quad (25)$$

Conversely, if one introduced  $\mathcal{F}$  in the usual manner, i.e., by starting with the asymptotic behavior of  $\phi_k$  written as

$$\phi_k(R) \xrightarrow{R \rightarrow \infty} \frac{i}{2k}[\mathcal{F}(k)e^{-ikR} - \mathcal{F}^*(k)e^{+ikR}], \quad (26)$$

one could identify  $A = \text{Re}(\mathcal{F})$  and  $B = -\text{Im}(\mathcal{F})$ , provided that both  $k$  and  $V(R)$  are real valued. Note that if one allows for a complex valued  $k$ , see [40], a fully general definition of the Jost function can be obtained by replacing  $\mathcal{F}^*(k)$  with  $\mathcal{F}(-k)$  in Eq. (26). In this article we use real and positive  $k$ , unless otherwise specified; when needed, we can allow  $k$  to be complex without any difficulty, because we restrict ourselves to the case of short-range interactions. We remark that our analysis of the  $S$  matrix in the previous section (done in the complex  $k$  plane) would be difficult to justify rigorously for the case of long-range interactions. However, as we shall see in this section, the approach based on the Jost function (for real argument  $k$ ) circumvents this obstacle, because it makes it possible to account for the NTR phenomenon without referring to the poles of the  $S$  matrix in the complex plane. Moreover, when it is possible to define the Jost function for complex  $k$ , it is easily seen that the two approaches are equivalent.

Regarding our preference for analyzing  $A(k)$  and  $B(k)$  instead of  $\mathcal{F}(k)$  itself, we point out that although the two solutions  $\chi_k^\pm(R) \sim e^{\pm ikR}$  are linearly independent in the strict sense, they will become linearly dependent in the limit  $k \rightarrow 0$  (from the numerical point of view) simply because  $e^{-ikR} \approx e^{ikR} \approx 1$  when  $kR \ll 1$ . Thus, it is desirable to replace  $\chi_k^\pm$  with a set of solutions which are more suitable at low  $k$ , namely  $f_k(R) \sim \sin(kR)$  and  $g_k(R) \sim \cos(kR)$ . Since we assume that  $\phi_k$ ,  $f_k$ ,  $g_k$  and  $\chi_k^\pm$  are exact solutions of the radial equation, the matching conditions (23) and (26) can be recast as equalities:  $k\phi_k = Af_k + Bg_k$ , and  $2ik\phi_k = \mathcal{F}^*\chi_k^+ - \mathcal{F}\chi_k^-$  respectively. As is well known, the Jost function can be expressed as  $\mathcal{F} = W[\chi_k, \phi_k]$ , where  $W[u, v] = uv' - u'v$  denotes the Wronskian. Similarly, for  $A$  and  $B$  we have  $A = W[g_k, \phi_k]$  and  $B = -W[f_k, \phi_k]$ , which can be used in practice to compute  $A(k)$  and  $B(k)$ .

We now shift our attention to the (normalized) physical solution  $\psi_k(R)$ , which is regular at  $R = 0$ . Hence, the physical and regular solutions only differ by a multiplicative constant, which can be easily found by comparing the asymptotic boundary condition obeyed by the physical solution [43],

$$\psi_k(R) \xrightarrow{R \rightarrow \infty} e^{i\delta} \sin(kR + \delta) = \frac{i}{2}(e^{-ikR} - e^{2i\delta}e^{ikR}), \quad (27)$$

to the asymptotic behavior in Eq. (26). Indeed, we find

$$\psi_k(R) = \frac{k}{\mathcal{F}(k)}\phi_k(R), \quad (28)$$

and we can also identify the  $S$  matrix,  $S = e^{2i\delta} = \mathcal{F}^*\mathcal{F}^{-1}$ . We recall the well known relationship between the phase shift  $\delta(k)$  in Eq. (27) and the Jost function; namely,  $\delta = -\arg(\mathcal{F})$ , which can also be written as  $\tan \delta = B/A$ , see Eqs. (23, 25, 27). Also note that if we make use of  $\mathcal{F} = |\mathcal{F}|e^{-i\delta}$ , then Eq. (25) can be expressed as  $A = |\mathcal{F}| \cos \delta$  and  $B = |\mathcal{F}| \sin \delta$ .

We emphasize that scattering resonances will affect strongly the  $k$  dependence of the normalization constant  $k[\mathcal{F}(k)]^{-1}$  in Eq. (28). Special attention has to be paid to the denominator  $\mathcal{F} = A - iB$ , which could vanish near  $k = 0$ , and thus produce a near threshold resonance. Hence, we proceed to analyze the low  $k$  behavior of the Jost function. Under the assumption of a



short-range potential, it is possible to expand  $A(k)$  and  $B(k)$  as power series. Indeed, given that the regular solution, as well as  $\cos(kR)$ , are analytic in  $k^2$  [44], and that  $\sin(kR)$  is analytic in  $k$  and is an odd function of  $k$ , we can write:

$$A(k) = A_0 + A_2 k^2 + A_4 k^4 + \dots \quad (29)$$

$$B(k) = B_1 k + B_3 k^3 + B_5 k^5 + \dots \quad (30)$$

For a finite-range potential, these power series can be rigorously deduced in a straightforward manner, and their validity can also be extended to the case of short-range potentials. However, for long-range potentials, e.g.,  $V(R) = -C_n/R^n$  for  $R \rightarrow \infty$ ,  $A(k)$  and  $B(k)$  are no longer analytic functions; their  $k$  dependence is rather complicated, as shown by Willner and Gianturco [45]. Nevertheless, even in the case of long-range interactions, both  $A(k)$  and  $B(k)$ , and hence  $\mathcal{F}(k)$  are generally well behaved, albeit nonanalytic; thus, we subscribe to the point of view advocated by Willner and Gianturco [45], that the low- $k$  expansion for the Jost function is simpler, more elegant, and more practical than the corresponding expression for  $\tan \delta(k)$  or the familiar effective range expansion for  $k \cot \delta(k)$ . We argue that one should employ the low- $k$  expansions for  $A(k)$  and  $B(k)$  of the Jost function  $\mathcal{F}(k) = A(k) - iB(k)$  rather than low  $k$  power series expansion of the phase shift (and all other physical quantities, such as the cross section). For example,

$$\tan \delta(k) = \frac{B(k)}{A(k)} = \frac{B_1 k + B_3 k^3 + \dots}{A_0 + A_2 k^2 + \dots}$$

should be kept as a fraction, rather than attempting to expand it consistently to  $O(k^2)$  or higher. Indeed, such an expansion would become unsuitable if  $A_0$  were vanishingly small, as its validity would be restricted to an extremely narrow range, namely  $k^2 \ll |A_0/A_2|$ , while the expression above remains valid and useful for a much wider range. Alternatively, we have

$$k \cot \delta = \frac{A_0 + A_2 k^2 + \dots}{B_1 + B_3 k^2 + \dots},$$

which could be expanded as a power series to give the familiar effective range expansion,

$$k \cot \delta \approx -\frac{1}{a} + \frac{r_{\text{eff}}}{2} k^2,$$

with  $a = -B_1/A_0$  the scattering length, and  $r_{\text{eff}} = 2(A_2/B_1 - A_0 B_3/B_1^2) = (2/B_1)(A_2 + B_3/a)$  the effective range. When  $A_0$  vanishes, we have  $a \rightarrow \pm\infty$  and  $r_{\text{eff}} \rightarrow 2A_2/B_1$ , and the effective range expansion remains valid, taking a simplified form:  $k \cot \delta \approx \frac{1}{2} r_{\text{eff}} k^2$ . However, if  $B_1$  is vanishingly small, we have  $a \approx 0$  and  $r_{\text{eff}} \rightarrow \pm\infty$ , and thus the effective range expansion is rendered useless.

We now analyze the elastic cross section in terms of the Jost function:

$$\sigma^{\text{elast}}(k) = \frac{\pi}{k^2} |1 - S(k)|^2,$$

where the  $S$  matrix is expressed as

$$S(k) = e^{2i\delta} = \frac{A + iB}{A - iB}.$$

Thus, the elastic cross section reads

$$\sigma^{\text{elast}}(k) = \frac{4\pi}{k^2} \frac{B^2(k)}{A^2(k) + B^2(k)}. \quad (31)$$

In the limit  $k \rightarrow 0$ , and provided that  $A(0) \neq 0$ , we recover the well known Wigner law for s-wave elastic scattering, which is simply the lowest order approximation,

$$\sigma^{\text{elast}} \xrightarrow[k \rightarrow 0]{} 4\pi \left( \frac{B_1}{A_0} \right)^2 = 4\pi a^2.$$

The domain of validity for Wigner's threshold law defines the so called Wigner regime; its extent is governed by the lowest order coefficients  $A_0$  and  $B_1$  in the Jost function expansions (29, 30). When neither  $A_0$  nor  $B_1$  is small, the Wigner regime will cover the entire low energy domain. Conversely, if either  $A_0$  or  $B_1$  is vanishingly small, Wigner's threshold law will be restricted to a narrow domain near  $k = 0$ , because the higher order terms in (29, 30) become dominant as  $k$  increases, and the  $k$ -dependence of the cross section in Eq. (31) changes dramatically.

Here, we are especially interested in the case of vanishingly small  $A_0$ , which corresponds to a NTR, and we establish the domain of validity for Wigner's law as follows: in Eq. (31) it is necessary that both  $A(k)$  and  $B(k)$  be replaced by Eqs. (29, 30) truncated to the lowest order, i.e., we require  $k \ll |A_0 A_2^{-1}|^{1/2}$  and  $k \ll |B_1 B_3^{-1}|^{1/2}$ . The former inequality is stronger than the latter, since  $B_1$  is typically finite when  $A_0 \rightarrow 0$ . Moreover, the  $B^2(k)$  term in the denominator of Eq. (31) has to remain negligible; hence, we impose yet another inequality,  $k \ll |A_0 B_1^{-1}| = |a|^{-1}$ , which is much stronger than either of the two inequalities above, and thus dictates the extent of the Wigner regime.

Since the Wigner regime is displaced towards extremely low energies when  $A_0 \approx 0$ , we need to analyze the behavior of the elastic cross section for the remainder of the low energy domain. Thus, we consider  $k$  outside the Wigner regime, but still inside the low energy domain, such that Eq. (30) can be truncated to the first term, and Eq. (29) to the second term. As  $k$  increases gradually,  $A_0$  becomes negligible compared to both  $A_2 k^2$  and  $B_1 k$ . Moreover, only the latter term survives, as we have  $|B_1|k \gg |A_2|k^2$  throughout the low energy domain. Consequently, the term  $A^2(k)$  in the denominator of Eq. (31) can be neglected entirely, and we recover the NTR-regime behavior,

$$\sigma^{\text{elast}}(k) \approx \frac{4\pi}{k^2}.$$

In summary, using the Jost function description, the elastic cross section can be parametrized in a simple way at low energy; namely, according to our discussion above, we keep only the relevant terms in Eqs. (29, 30) to approximate Eq. (31) as

$$\sigma^{\text{elast}}(k) = 4\pi \frac{B_1^2}{A_0^2 + B_1^2 k^2} = 4\pi \frac{1}{k^2 + (1/a)^2}, \quad (32)$$

where  $a = -B_1/A_0$  is the full scattering length. The simple expression above makes it clear that the gradual transition

from Wigner's threshold law to the NTR-regime behavior takes place near  $k \approx |a|^{-1}$ , where the two terms in the denominator are comparable. We remark that Eq. (32) is in agreement with Eq. (10) obtained in the previous section using the pole factorization of the  $S$  matrix, and we shall discuss their equivalence in Sec. 6.

### 5.2. Multi-channel case

In the case of  $N$  coupled channels, the regular solution  $\Phi$  is an  $N \times N$  matrix with elements  $\phi_{ij}$  satisfying the system of coupled radial equations,

$$\frac{d^2}{dR^2}\Phi(\mathbf{k}, R) + \mathbf{K}^2\Phi(\mathbf{k}, R) = \frac{2\mu}{\hbar^2}\mathbf{V}(R)\Phi(\mathbf{k}, R), \quad (33)$$

with  $\mathbf{k} \equiv (k_1, k_2, \dots, k_N)$  and  $k_n = \sqrt{2\mu(E - \varepsilon_n)/\hbar^2}$  the momenta corresponding to channel threshold energies  $\varepsilon_n$ . For simplicity we consider all channels open, with all  $k_n$  real valued and  $k_n > 0$ .  $\mathbf{K}$  is a diagonal matrix with elements  $k_n\delta_{nm}$ , while  $\mathbf{V}(R)$  is a full matrix containing the couplings  $V_{nm}(R)$ . Note that the diagonal elements of  $\mathbf{V}$  also include centrifugal terms of the form  $\ell_n(\ell_n + 1)R^{-2}$ .

The regular solution is uniquely specified by initial-value type conditions at  $R = 0$ ,

$$\phi_{nm}(R) \xrightarrow{R \rightarrow 0} \delta_{nm}R^{\ell_n+1}.$$

Assuming that the coupling matrix  $\mathbf{V}$  is real, we extract two real valued matrices ( $\mathbf{A}$  and  $\mathbf{B}$ ) from the asymptotic behavior of the regular solution,

$$\Phi \xrightarrow{R \rightarrow \infty} \mathbf{K}^{-\ell-1}(\mathbf{jA} + \mathbf{nB}),$$

where  $\mathbf{K}^{-\ell-1} = \text{diag}\{k_n^{-\ell_n-1}\}$ , and the diagonal matrices  $\mathbf{j}$  and  $\mathbf{n}$  contain the free solutions, i.e., the Riccati-Bessel functions  $j_\ell(k_n R)$  and  $n_\ell(k_n R)$  for each channel. Note that, although the asymptotic behavior in the last equation was written in matrix notation, the coefficients  $A_{nm}$  and  $B_{nm}$  (i.e., the matrix elements of  $\mathbf{A}$  and  $\mathbf{B}$ ) are extracted independently for each pair of indices  $(n, m)$ . Indeed, for each component  $(n)$  of any column solution  $(m)$  contained in  $\Phi$ , we write the asymptotic behavior explicitly,

$$k_n^{\ell_n+1}\phi_{nm}(R) \xrightarrow{R \rightarrow \infty} A_{nm}j_{\ell_n}(k_n R) + B_{nm}n_{\ell_n}(k_n R).$$

Employing this matching condition for  $\phi_{nm}$  (together with a similar equation for  $d\phi_{nm}/dR$ ) at  $R = R_{\max}$  in the asymptotic region, we obtain

$$A_{nm} = -k_n^{\ell_n}W[\phi_{nm}, n_{\ell_n}] \quad (34)$$

$$B_{nm} = +k_n^{\ell_n}W[\phi_{nm}, j_{\ell_n}] \quad (35)$$

where  $W[\dots]$  stands for the Wronskian. The Jost matrix is defined in terms of the matrices  $\mathbf{A}$  and  $\mathbf{B}$  as

$$\mathbf{F} = \mathbf{A} - i\mathbf{B}, \quad (36)$$

which is a direct generalization of Eq. (25). The factor  $k_n^{\ell_n+1}$  in the equations above was used for convenience, such that the

Jost matrix is well behaved when  $k_n \rightarrow 0$ . In this paper we restrict our discussion to s-wave scattering, i.e.,  $\ell = 0$  in the entrance channel; note that only the centrifugal term in the entrance channel is relevant for analyzing the threshold behavior. The values of  $\ell_n$  in all other channels can be arbitrary (as allowed by the specifics of any given scattering problem). However, we set  $\ell_n = 0$  in all channels to simplify our notation; thus, the asymptotic behavior of the regular solution reads

$$k_n\phi_{nm}(R) \xrightarrow{R \rightarrow \infty} A_{nm}\sin(k_n R) + B_{nm}\cos(k_n R),$$

which is identical to the single channel version, see Eq. (23). Equivalently, the asymptotic behavior of  $\Phi$  can be written in terms of Jost matrix elements  $F_{nm} = A_{nm} - iB_{nm}$  as

$$\frac{2}{i}k_n\phi_{nm}(R) \xrightarrow{R \rightarrow \infty} e^{-ik_n R}F_{nm} - e^{+ik_n R}F_{nm}^*,$$

where  $F_{nm}^* = A_{nm} + iB_{nm}$  is the complex conjugate of  $F_{nm}$ .

The normalized (physical) solution  $\Psi$  can be written in terms of the regular solution  $\Phi$ ,

$$\Psi(R) = \Phi(R)\mathbf{F}^{-1}\mathbf{K}, \quad (37)$$

and it has the well known asymptotic behavior,

$$\psi_{nm}(R) \xrightarrow{R \rightarrow \infty} \frac{i}{2} \left[ e^{-ik_n R} \delta_{nm} - e^{+ik_n R} (k_n^{-1/2} S_{nm} k_m^{1/2}) \right], \quad (38)$$

where  $S_{nm}$  are the elements of the  $S$  matrix,

$$\mathbf{S} = \mathbf{K}^{-1/2}(\mathbf{F})^*(\mathbf{F})^{-1}\mathbf{K}^{1/2}. \quad (39)$$

Equations (37) and (39) contain the inverse of the Jost matrix, which we write explicitly as

$$\mathbf{F}^{-1} = \frac{1}{\det(\mathbf{F})} [\text{Cof}(\mathbf{F})]^T, \quad (40)$$

with  $[\text{Cof}(\mathbf{F})]^T$  the transpose of the matrix of cofactors of  $\mathbf{F}$ , and  $\det(\mathbf{F})$  the determinant of  $\mathbf{F}$ .

As in the single-channel case, we focus our attention on the denominator, i.e., the determinant of the Jost matrix. We are interested in the situation when  $\det(\mathbf{F})$  is vanishingly small, such that the scattering cross sections are resonantly enhanced; if  $T_{nm}$  are the elements of the  $T$  matrix,  $\mathbf{T} = \mathbf{1} - \mathbf{S}$ , we have

$$\sigma(n \leftarrow m) \sim \frac{\pi}{k_m^2} |T_{nm}|^2 \sim |\det(\mathbf{F})|^{-2}.$$

Although the determinant of the Jost matrix cannot vanish on the real axis [46], it can *almost* reach zero. Also, recall that we only consider the case of a scattering problem without closed channels, thus eliminating the possibility of Feshbach resonances. Therefore, by extrapolation from the single-channel case, the only remaining possibility is that of a potential resonance at low energy; such a resonance would correspond to a quasi-bound state near the threshold of the channel with the highest energy asymptote, which we take as our entrance channel ( $n = 1$ ). For clarity, we assume  $E > \varepsilon_1 > \varepsilon_2 > \dots > \varepsilon_n > \dots > \varepsilon_N$ .

When  $\det(\mathbf{F}) \approx 0$  at a channel threshold, the factor  $|\det(\mathbf{F})|^{-2}$  in the equation above will be responsible for a resonance enhancement, and will also affect the threshold behavior of cross sections. We now give a detailed analysis of a NTR in the entrance channel,  $n = 1$ , and we start by using a cofactor expansion of the determinant along the first row,

$$\det(\mathbf{F}) = \sum_{m=1}^N F_{1m} C_{1m}, \quad (41)$$

where  $C_{1m}$  is the cofactor corresponding to the element  $(1, m)$ . Next, we extract  $C_{11}$  outside the sum, and we isolate the first term (i.e., the diagonal element  $F_{11}$ ) to recast  $\det(\mathbf{F})$  as

$$\det(\mathbf{F}) = C_{11} (F_{11} + f_{11}), \quad (42)$$

where

$$f_{11} \equiv \frac{1}{C_{11}} \sum_{m \neq 1} F_{1m} C_{1m}. \quad (43)$$

Separating the real and imaginary parts of the last factor in Eq. (42), namely  $F_{11} + f_{11} = \mathcal{A} - i\mathcal{B}$ , and defining

$$D \equiv |F_{11} + f_{11}|^2 = \mathcal{A}^2 + \mathcal{B}^2,$$

we can write

$$|\det(\mathbf{F})|^2 = |C_{11}|^2 |\mathcal{A} - i\mathcal{B}|^2 = |C_{11}|^2 D. \quad (44)$$

Under the assumption that  $f_{11}$  is suitably small, and provided that  $C_{11} \neq 0$ , only the factor  $D \approx |F_{11}|^2 = A_{11}^2 + B_{11}^2$  can be responsible for NTRs. In order to clarify these assumptions, we recall that, as we explained in Sec. 4, due to the coupling of the entrance channel with other open channels, the resonance pole will be pushed away from the threshold; thus, in the limit of strong coupling, the existence of a near threshold resonance will become highly unlikely. Conversely, the appearance of a prominent NTR requires the entrance channel be weakly coupled to all other open channels. To simplify, one can use a coupling strength parameter  $\lambda$  to redefine these particular couplings ( $V_{1n} = V_{n1} \rightarrow \lambda V_{n1}$ ) which will become vanishingly small when  $\lambda \rightarrow 0$ . Hence, we assume the regular solution matrix  $\Phi$  is *almost* block diagonal, with a small  $1 \times 1$  block containing  $\phi_{11}$  and a large  $(N-1) \times (N-1)$  block corresponding to all other open channels. The remaining elements, i.e.,  $\phi_{1m}$  with  $m \neq 1$  in the first row, and  $\phi_{n1}$  with  $n \neq 1$  in the first column are vanishingly small when  $\lambda \rightarrow 0$ . Consequently, from Eqs. (34, 35, 36) we have (for  $n \neq 1$ )  $F_{n1} = \mathcal{O}(\lambda)$  when  $\lambda \rightarrow 0$ , and thus  $C_{1m} = \mathcal{O}(\lambda)$  for  $m \neq 1$ . Note that  $C_{11}$  is independent of  $\lambda$  in zeroth order, and hence we assume  $C_{11} = \mathcal{O}(1)$ . Finally, we also have  $F_{1m} = \mathcal{O}(\lambda)$  for  $m \neq 1$ , and from Eq. (43) we have  $f_{11} = \mathcal{O}(\lambda^2)$  when  $\lambda \rightarrow 0$ .

Regarding the caveat of an accidental vanishing of  $C_{11}$  near the threshold of the entrance channel, recall that in the limit  $\lambda \rightarrow 0$  the channel  $n = 1$  becomes decoupled from the remaining  $N-1$  channels, and we have  $\lim_{\lambda \rightarrow 0} C_{11} = \det[\mathbf{F}^{(N-1)}]$ , where  $\mathbf{F}^{(N-1)}$  is the Jost matrix for the scattering problem with  $N-1$  channels. Thus,  $\det[\mathbf{F}^{(N-1)}]$  cannot be vanishingly small for collision energies  $E > \varepsilon_1$ , since  $E$  is very high above  $\varepsilon_2$

(which is the highest threshold for the scattering problem with  $N-1$  channels). Indeed, as we assume  $\varepsilon_1 - \varepsilon_2$  is much larger than the generic low-energy scale of the scattering problem; thus, it is safe to factor out  $C_{11} = \mathcal{O}(1)$  as a background contribution, as we already anticipated in the equations above.

Denoting  $k = k_1$ , we now focus on the  $k$  dependence of  $D(k)$  in Eq. (44), which stems from the behavior of  $F_{11}(k)$  and  $f_{11}(k)$ . We emphasize that all quantities are analyzed as functions of the single variable  $k$ . All other momenta, i.e.,  $k_n$  for channels  $n = 2, 3, \dots, N$ , can be easily expressed in terms of the entrance channel momentum: using  $k_n^2 = 2\mu(E - \varepsilon_n)$ , we write

$$k_n = \sqrt{\Delta_n + k^2},$$

with  $\Delta_n = 2\mu(\varepsilon_1 - \varepsilon_n)$ . In the ultracold limit ( $k \rightarrow 0$ ) we have  $k^2 \ll \Delta_n$  for all  $n \neq 1$ , and we use a power series expansion:

$$k_n(k^2) \approx \sqrt{\Delta_n} + \mathcal{O}(k^2).$$

Moreover, the regular solution  $\Phi$  is a function of  $k^2$  (rather than  $k$  itself), and we deduce from Eqs. (34, 35) that except for the first row, all matrix elements  $A_{nm}$  and  $B_{nm}$  are also functions of  $k^2$ . Thus, when  $k \rightarrow 0$  we have

$$F_{nm}(k^2) = F_{nm}(0) + \mathcal{O}(k^2), \quad \text{for } n \neq 1,$$

Similarly, the cofactors corresponding to the first row of  $\mathbf{F}$  can be written as

$$C_{1m}(k^2) = C_{1m}(0) + \mathcal{O}(k^2), \quad \text{for all } m,$$

which ensures that the ratios  $c_m \equiv C_{1m}/C_{11}$  in Eq. (43) can be expanded in a similar fashion:

$$c_m(k^2) = c_m(0) + \mathcal{O}(k^2).$$

Rewriting Eq. (43) as

$$f_{11} = \sum_{m \neq 1} F_{1m} c_m, \quad (45)$$

and separating its real and imaginary parts, we have

$$\text{Re}(f_{11}) = \sum_{m \neq 1} [A_{1m}(k) \text{Re} c_m(k) + B_{1m}(k) \text{Im} c_m(k)], \quad (46)$$

$$\text{Im}(f_{11}) = \sum_{m \neq 1} [A_{1m}(k) \text{Im} c_m(k) - B_{1m}(k) \text{Re} c_m(k)]. \quad (47)$$

In these equations, special attention has to be paid to  $A_{1m}(k)$  and  $B_{1m}(k)$ . From Eqs. (34, 35) we obtain the expansions:

$$A_{1m}(k) = A_{1m}(0) + k^2 A_{1m}^{(2)} + \mathcal{O}(k^4), \quad (48)$$

$$B_{1m}(k) = k B_{1m}^{(1)} + k^3 B_{1m}^{(3)} + \mathcal{O}(k^5). \quad (49)$$

Since the series of  $B_{1m}(k)$  contains odd powers, and  $c_m(k)$  in Eq. (45) are complex quantities, the power series in Eqs. (46, 47) contain both odd and even powers of  $k$ ,

$$\text{Re}(f_{11}) = a(0) + k a^{(1)} + k^2 a^{(2)} + \mathcal{O}(k^3), \quad (50)$$

$$\text{Im}(f_{11}) = b(0) + k b^{(1)} + k^2 b^{(2)} + \mathcal{O}(k^3). \quad (51)$$

Thus, the power series of  $\mathcal{A}(k)$  and  $\mathcal{B}(k)$  will also contain all possible terms, i.e., both odd and even powers:

$$\mathcal{A}(k) = \mathcal{A}_0 + k\mathcal{A}_1 + k^2\mathcal{A}_2 + \dots, \quad (52)$$

$$\mathcal{B}(k) = \mathcal{B}_0 + k\mathcal{B}_1 + k^2\mathcal{B}_2 + \dots \quad (53)$$

The coefficients  $\mathcal{A}_v$  and  $\mathcal{B}_v$  will be expressed in terms of  $A_{1m}^{(v)}$ ,  $B_{1m}^{(v)}$ ,  $a^{(v)}$  and  $b^{(v)}$ . Indeed, recall that  $\mathcal{A} = \text{Re}(F_{11} + f_{11}) = A_{11} + \text{Re}(f_{11})$  and  $\mathcal{B} = -\text{Im}(F_{11} + f_{11}) = B_{11} - \text{Im}(f_{11})$ . From the equations above, we obtain for the coefficients up to order  $v = 2$ ,

$$\mathcal{A}_0 = \mathcal{A}(0) = a(0) + A_{11}(0)$$

$$\mathcal{A}_1 = a^{(1)}$$

$$\mathcal{A}_2 = a^{(2)} + A_{11}^{(2)}$$

and

$$\mathcal{B}_0 = \mathcal{B}(0) = -b(0)$$

$$\mathcal{B}_1 = -b^{(1)} + B_{11}^{(1)}$$

$$\mathcal{B}_2 = -b^{(2)}.$$

Under the assumption of weak coupling ( $\lambda \rightarrow 0$ ), we have  $f_{11} = O(\lambda^2) \rightarrow 0$ . Thus, all  $a^{(v)}$  and  $b^{(v)}$  are negligibly small; however, their presence in the equations above is necessary, because they limit the effects caused by near threshold resonances. Indeed, note that  $\mathcal{A}_0$  and  $\mathcal{B}_0$  cannot vanish simultaneously; in other words, one cannot have:  $A_{11}(0) = 0$  and  $a(0) = 0$  and  $b(0) = 0$ . Were that the case,  $D(k)$  and hence  $\det(\mathbf{F})$  would vanish at  $k = 0$ , which is impossible (as we mentioned earlier). Nevertheless, when  $\lambda$  is small, so are  $a(0)$  and  $b(0)$ . Also, as in the single-channel case, it is possible that  $A_{11}(0) \approx 0$ . Thus, although the quantity  $D(k = 0) = \mathcal{A}_0^2 + \mathcal{B}_0^2$  cannot vanish, it could reach very small values (which is the signature of NTR).

Finally, we analyze the threshold behavior of cross sections in the presence of a NTR; from Eqs. (39, 40) we obtain

$$S_{nm} = \delta_{nm} + \sqrt{\frac{k_m}{k_n}} \frac{2i \sum_j B_{nj} C_{mj}}{\det(\mathbf{F})}.$$

We only consider scattering from the ultracold channel  $m = 1$  to all final channels  $n = 1, 2, 3, \dots, N$ ; thus, using the notation  $k = k_1$ , the cross sections read

$$\sigma(n \leftarrow 1) \sim \frac{\pi}{k^2} |T_{n1}(k)|^2 \sim \frac{|\sum_j B_{nj} C_{1j}|^2}{kk_n |C_{11}|^2 D(k)}.$$

Except for  $D(k)$ , all other quantities are finite when  $k \rightarrow 0$ , and can be replaced by their values at  $k = 0$ , i.e.,  $B_{nj}(0)$ ,  $C_{1j}(0)$ ,  $C_{11}(0)$  and  $k_n(0)$ , which amount to an overall ( $n$  dependent) constant. This allows us to simplify the expression above; for reactive (or inelastic) scattering,  $n \neq 1$ , we obtain

$$\sigma^{\text{react}}(n \leftarrow 1) \sim \frac{\text{const}(n)}{D(k)} k^{-1}, \quad (54)$$

while for elastic scattering, we have  $k_n = k$  and  $B_{1j}(k) \sim k$ , and the cross section reads

$$\sigma^{\text{elast}}(1 \leftarrow 1) \sim \frac{\text{const}'}{D(k)}. \quad (55)$$

Recall  $D(k) = \mathcal{A}^2(k) + \mathcal{B}^2(k)$ , which is expanded at low  $k$ ,

$$D(k) = D_0 + kD_1 + k^2D_2 + \dots, \quad (56)$$

with

$$D_0 = D(0) = [b(0)]^2 + [a(0) + A_{11}(0)]^2,$$

$$D_1 = 2[-b(0)\mathcal{B}_1 + a^{(1)}\mathcal{A}_0],$$

$$D_2 = \mathcal{B}_1^2 + [a^{(1)}]^2 + 2[\mathcal{A}_0\mathcal{A}_2 + b(0)b^{(2)}].$$

As argued above,  $D_0$  cannot vanish identically; however,  $D_0$  is small in the case of a NTR, and hence it is the most important parameter characterizing the NTR. Note that the first order term in Eq. (56) can be neglected when both the weak coupling ( $\lambda \rightarrow 0$ ) assumption and the NTR assumption ( $A_{11}(0) \approx 0$ ) are valid; indeed, we have  $D_1 \approx -2b(0)\mathcal{B}_1^{(1)} = O(\lambda)$ . Thus, even for a pronounced NTR, i.e., when  $D_0$  approaches its minimum value,  $D_0 \approx D_{\min} \approx [b(0)]^2 = O(\lambda^2)$ , the linear term will become negligible compared to  $D_0$  for  $k \ll D_0/|D_1| \approx |b(0)/\mathcal{B}_1^{(1)}|$ . In the ultracold limit ( $k \rightarrow 0$ ) the quadratic term in Eq. (56) can be neglected as well; specifically, the requirement is  $k \ll \sqrt{D_0/D_2}$ . Making use of the approximations  $D_0 \approx [b(0)]^2$  and  $D_2 \approx [\mathcal{B}_1^{(1)}]^2$ , we have  $\sqrt{D_0/D_2} \approx |b(0)/\mathcal{B}_1^{(1)}|$ . Hence, the strong inequality  $k \ll \sqrt{D_0/D_2}$  defines the Wigner regime, since we can ignore both the linear and quadratic terms in Eq. (56). Indeed, we have  $D(k) \approx D_0$ , and we recover Wigner's threshold laws:  $\sigma^{\text{react}} \sim k^{-1}$  and  $\sigma^{\text{elast}} \approx \text{constant}$ .

The linear term in Eq. (56) can also be neglected outside the Wigner regime, i.e., for the remainder of the low  $k$  domain; indeed, when  $k \gg |b(0)/\mathcal{B}_1^{(1)}|$ , we have  $k^2D_2 \gg kD_1$  and also  $k^2D_2 \gg D_0$ , which ensures that  $D(k) \approx k^2D_2$ . Thus, discarding the linear term altogether in Eq. (56), we simplify Eqs. (54) and (55), and we obtain

$$k^{0,1} \sigma^{\text{elast, react}} \sim \frac{1}{D_0 + k^2D_2}, \quad (57)$$

where the prefactors  $k^0 = 1$  and  $k$  correspond to elastic and reactive scattering, respectively. We emphasize that this expression is a good approximation throughout the entire low- $k$  regime, and despite its simplicity, it accounts for the combined Wigner and NTR-regime behavior. For reactive scattering we have

$$\sigma^{\text{react}} \sim \begin{cases} k^{-1}, & \text{Wigner regime for } k \ll \sqrt{D_0/D_2} \\ k^{-3}, & \text{NTR regime for } k \gg \sqrt{D_0/D_2}, \end{cases}$$

while for elastic scattering,

$$\sigma^{\text{elast}} \sim \begin{cases} k^0, & \text{Wigner regime} \\ k^{-2}, & \text{NTR regime,} \end{cases}$$

According to Eq. (57) there is a smooth transition between the two types of behavior (Wigner and NTR) which takes place around  $k = \sqrt{D_0/D_2}$ , where all three terms in Eq. (56) are comparable. Thus, the linear term in Eq. (56) only plays a minor role near the transition, while becoming negligible for both Wigner and NTR regimes.

We remark that when the coupling strength  $\lambda$  increases, and the system becomes more reactive,  $a^{(v)}$  and  $b^{(v)}$  will increase;



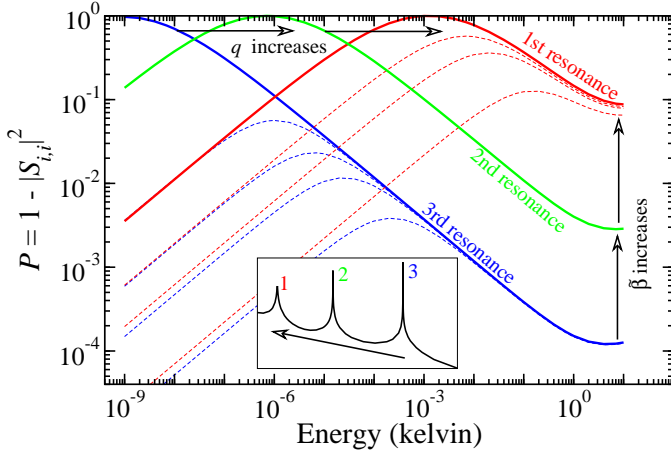


Figure 12: Comparison of reaction probabilities for the resonances of  $\text{H}_2 + \text{Cl}$ . The imaginary part of the scattering length ( $\beta$ , see Fig. 3) is shown in the inset to help identify the resonances. The three solid curves correspond to the three critical values of  $m$  (for the first, second and third resonance, which are shown in red, green and blue, respectively). The dashed curves correspond to values of  $m$  near the first and third resonance. The arrows indicate the increase of reactivity, and the increase of  $\beta$  and  $q$ , as  $m$  decreases.

hence,  $D_0$  and  $D_1$  will become large (even if  $A_0 \approx 0$  still holds) and the NTR regime will be pushed to higher values of  $k$ , where higher-order terms will become dominant. Eventually, the signature of the NTR will disappear, as suggested in Fig. 12, which shows that for the lowest reactivity  $\beta$  corresponding to the third resonance, the pole is located at very low  $k$ , and the NTR regime extends to a sizable range for larger  $k$ . The extent of the NTR regime is smaller for the second resonance corresponding to a larger  $\beta$ , and smaller still for the first resonance with the largest reactivity  $\beta$ . Thus, in the limit of strong coupling, the very existence of a quasi-bound state of the atom-dimer complex becomes unlikely, since such a complex will be short lived; consequently, NTRs cannot exist (or are less pronounced) for highly reactive systems.

## 6. Equivalence between different approaches

In the case of purely elastic scattering (single channel), the equivalence of the two approaches is based on the simple relationship between the  $S$  matrix and the Jost function, see Eq. (7). The expressions (8) and (29, 30) merely give different parametrizations for the  $S$  matrix, and hence for the elastic cross section. To elucidate their equivalence, we first note that the pole factorization (8) relies on the power series expansion of the Jost function around its zero (at  $k = p$ ). Recall that we assume a short range potential, such that  $\mathcal{F}(k)$  is analytic in the entire complex  $k$  plane, or at least inside a wide region containing the threshold  $k = 0$ . We thus write

$$\mathcal{F}(k) = \sum_{n=1}^{\infty} F_n (p - k)^n,$$

where the coefficients  $F_n$  are complex numbers. The absence of the term for  $n = 0$  in the sum above makes it explicit that  $\mathcal{F}(p) = 0$ , and allows for the factorization  $\mathcal{F}(k) = (p - k)\tilde{\mathcal{F}}(k)$ .

The background contribution  $\tilde{\mathcal{F}}(k)$  is also analytic, and assuming it to be slowly varying within a small domain containing both  $k = p$  and  $k = 0$ , we can truncate its power series in the low energy domain:

$$\tilde{\mathcal{F}}(k) \approx \tilde{\mathcal{F}}_0 + \tilde{\mathcal{F}}_1 k.$$

Note that for  $\tilde{\mathcal{F}}(k)$  we employ a power series expansion around  $k = 0$ , which is more convenient. Hence, the  $S$  matrix reads

$$S(k) = \frac{\mathcal{F}(-k)}{\mathcal{F}(k)} = \frac{p + k}{p - k} \frac{\tilde{\mathcal{F}}(-k)}{\tilde{\mathcal{F}}(k)},$$

and we recognize the background contribution, see Eq. (8),

$$\tilde{S}(k) = \frac{\tilde{\mathcal{F}}(-k)}{\tilde{\mathcal{F}}(k)},$$

which is slowly varying near  $k = 0$ , due to the smooth behavior of  $\tilde{\mathcal{F}}(k)$ . Truncating the power series of  $\tilde{S}$  to first order, we have  $\tilde{S}(k) \approx 1 - 2i\tilde{a}k$ . The unitarity of  $\tilde{S}$  on the real axis ensures that the coefficient of the first order term in this expansion is purely imaginary, and we have used the customary notation, namely the background scattering length  $\tilde{a}$ . Thus, in the pole factorization approach, the full  $S$  matrix at low  $k$  reads

$$S(k) \approx \frac{p + k}{p - k} (1 - 2i\tilde{a}k).$$

We now compare this result with the equivalent expression obtained in the explicit Jost function approach, namely in terms of  $\mathcal{F}(k) = A(k) - iB(k)$ . We emphasize that  $A(k)$  and  $B(k)$  are expanded in power series around  $k = 0$  only, and we remark that for a short range potential, the power series of  $A(k)$  and  $B(k)$  remain valid when  $k$  takes complex values; moreover, the expansion coefficients  $A_n$  and  $B_n$  in Eqs. (29, 30) remain real numbers. Therefore, if a zero of the Jost function (i.e., a pole of the  $S$  matrix) is located on the imaginary axis,  $p = i\kappa$ , then  $\kappa$  is a real valued solution of the equation

$$A_0 + B_1\kappa - A_2\kappa^2 - B_3\kappa^3 + \dots = 0,$$

with all coefficients real. In the case of a NTR,  $A_0$  is vanishingly small, and to a good approximation we have

$$\kappa \approx -\frac{A_0}{B_1} = \frac{1}{a},$$

where  $a$  is the full scattering length, which agrees with Eq. (11). As we discussed in Sec. 5.1, the  $S$  matrix is simply written as

$$S(k) = \frac{A_0 + iB_1k + A_2k^2 + \dots}{A_0 - iB_1k + A_2k^2 - \dots}.$$

When the resonance pole  $p = i\kappa$  is very close to  $k = 0$ , this expression truncated to second order becomes equivalent with the similar expression from the pole factorization approach, which has the advantage of using the exact value of the resonance pole (extracted as a fitting parameter from the computed scattering cross section, as it was done in Sec. 4). However, for complex  $k$ , the very definition of the  $S$  matrix becomes problematic, as

it imposes strict requirements for the asymptotic behavior of the interaction potential. Hence, the direct approach based on Jost functions for real  $k$  has the advantage of being fully general. We also emphasize that the Jost function has a smooth  $k$ -dependence, and it can be easily interpolated on a rather coarse  $k$ -mesh, which is very convenient in practice; nevertheless, this advantage has remained largely overlooked, despite being recognized more than four decades ago by Heller and Reinhardt [47].

Regarding the coupled-channel case, we remark that Eq. (57) obtained in the Jost function approach represents a parametrization which is identical to Eq. (17) from the pole factorization treatment, provided we simplify the latter to read  $k\sigma^{\text{react}}(k) = 4\pi q(k^2 + |p|^2)^{-2}$ . We can thus identify  $D_0/D_2 = |p|^2 = q^2 + \kappa^2$  in the denominator, and we regard  $q$  in the numerator as an overall measure of background reactivity (due to the couplings  $V_{n1} = V_{1n}$  between the entrance channel and all other channels).

## 7. Qualitative interpretation based on the wave function amplitude

A very simple picture emerges from the treatment using the Jost function; indeed, as noted for the single-channel discussion in Sec. 5.1, the amplitude of the physical wave function is modulated by the inverse of the Jost function  $\mathcal{F}^{-1}(k)$ , see Eq. (28). This scaling property is especially useful in the low energy domain, i.e., for  $k \lesssim |\tilde{a}|^{-1}$ , when the regular solution in the *short range* ( $R \lesssim |\tilde{a}|$ ) region is nearly  $k$ -independent:  $\phi_k(R) \approx \phi_0(R)$ . Hence, within the short-range region, Eq. (28) reads  $\psi_k(R) \approx k\mathcal{F}^{-1}(k)\phi_0(R)$ , and the  $k$  dependence of the physical solution is driven entirely by the scaling factor  $k\mathcal{F}^{-1}(k)$ .

In the absence of NTRs, the Jost function can also be replaced by its value at  $k = 0$ ,  $\mathcal{F}(0) = A_0$ , and we obtain the well known linear scaling of the short-range amplitude of the physical wave function,  $\psi_k(R) \approx kA_0^{-1}\phi_0(R)$ , characteristic to the Wigner regime. However, when  $\mathcal{F}(0) = A_0$  is vanishingly small, it produces a resonance enhancement for  $\psi_k(R)$ , and also the anomalous NTR behavior,

$$|\psi_k(R)|^2 \approx \frac{k^2}{A_0^2 + B_1^2 k^2} |\phi_k(R)|^2. \quad (58)$$

We remark that this simple expression for the single-channel case already contains the main result, Eq. (57), obtained rigorously in Sec. 5.2 for the coupled-channel case. This can be justified qualitatively, if we rely on the following physical argument; under the assumption of small couplings, the entrance-channel component ( $\psi_1$ ) of the physical wave function follows the same scaling as in the single-channel case, see Eq. (37). This  $k$ -dependence in the equation above will be imprinted (via the couplings  $V_{nm}$ ) on all the other components  $\psi_n$ . Although the entrance-channel component obeys Eq. (58) only at short range, all other components will obey it for all  $R$  (including the long-range region). Thus, according to Eq. (38) for  $m = 1$ , we extract the matrix elements  $S_{n1}$  from the asymptotic behavior

of  $\psi_n(R)$ , and we obtain for  $n \neq 1$

$$\frac{k}{k_n} |S_{n1}|^2 \propto |\psi_n|^2 \propto \frac{k^2}{A_0^2 + B_1^2 k^2},$$

where we used  $k = k_1$  for the entrance channel, and  $k_n(k) \approx \sqrt{\Delta_n}$  is constant. Finally, we obtain for the reaction cross section,

$$k\sigma^{\text{react}}(n \leftarrow 1) \propto \frac{1}{A_0^2 + B_1^2 k^2},$$

which is the same result obtained in Eq. (57), with  $D_0 \approx A_0^2$  and  $D_2 \approx B_1^2$ .

## 8. Conclusions

In conclusion, we found that a near threshold resonance will affect dramatically the behavior of the  $s$ -wave cross section at low energy. In fact, the low energy domain will be divided in two distinct regimes: the Wigner regime with the well known scaling ( $\sigma^{\text{react}} \propto k^{-1}$ ) and the NTR regime with the anomalous scaling  $\sigma^{\text{react}} \propto k^{-3}$ . We derived simple analytical expressions for both elastic and reaction (inelastic) cross sections, which depend on the position of the pole of the  $S$  matrix, and found very good agreement with results obtained numerically for the full reactive scattering problem. We explained the anomalous NTR-regime behavior using two different approaches—one based on the pole factorization of the  $S$  matrix, and a more general treatment based on the low energy expansion of the Jost function.

We remark that the  $k^{-3}$  NTR-regime behavior (for  $s$ -wave) is a general feature, and it can be a rather common occurrence in scattering problems; however, unless the resonance pole is very close to  $k = 0$ , the presence of the NTR can be somewhat inconspicuous, or it can be masked by higher partial wave contributions. Although previous work hinted at such anomalous resonant behavior—which was explored either by using mass-scaling [33, 48], or external fields [49]—the new NTR-regime behavior shown in Eq. (15) was discussed only recently [24]. These studies explored the effects of mass-scaling or magnetic field scanning at fixed scattering energy, e.g., see [50]. In our work, we revealed the effect of NTRs in two benchmark atom-diatom reactive scattering systems by mass-scaling ( $\text{H}_2 + \text{Cl}$  and  $\text{H}_2 + \text{F}$ ), but it also appears in any system with a zero-energy resonance, such as in photoassociation at ultralow temperatures [51, 52], ultracold collisions in general [53], or spin-relaxation in ultracold atomic samples [54]. The modified ( $k^{-3}$ ) behavior of the reaction (inelastic) cross section will play a role in the interpretation of experiments such as [20], and also for theories based on Wigner's threshold law developed to account for resonances in ultracold molecular systems [17].

This work was partially supported by the US Department of Energy, Office of Basic Energy Sciences (RC), and the Army Research Office Chemistry Division (I. S.).

## References

- [1] C. Chin, R. Grimm, P. Julienne, and E. Tiesinga, Rev. Mod. Phys. **82**, 1225 (2010).

- [2] M. H. G. de Miranda, A. Chotia, B. Neyenhuis, D. Wang, G. Quémener, S. Ospelkaus, J. L. Bohn, J. Ye, and D. S. Jin, *Nature Phys.* **7**, 502 (2011).
- [3] J. N. Byrd, J. A. Montgomery, Jr., and R. Côté, *Phys. Rev. Lett.* **109**, 083003 (2012).
- [4] F. Dalfovo, S. Giorgini, L. P. Pitaevskii, and S. Stringari, *Rev. Mod. Phys.* **71**, 463 (1999); A. J. Leggett, *Rev. Mod. Phys.* **73**, 307 (2001).
- [5] S. Giorgini, L. P. Pitaevskii, and S. Stringari, *Rev. Mod. Phys.* **80**, 1215 (2008).
- [6] T. Kraemer, M. Mark, P. Waldburger, J. G. Danzl, C. Chin, B. Engeser, A. D. Lange, K. Pilch, A. Jaakkola, H.-C. Nägerl, and R. Grimm, *Nature* **440**, 315 (2006).
- [7] L. Carr, D. DeMille, R. Krems, and J. Ye, *New J. Phys.* **11**, 055049 (2009).
- [8] O. Dulieu, R. Krems, M. Weidemüller, and S. Willitsch, *Phys. Chem. Chem. Phys.* **13**, 18703 (2011).
- [9] D. S. Jin and J. Ye, *Chem. Rev.* **112**, 4801 (2012), and references therein.
- [10] R. Côté and A. Dalgarno, *J. Mol. Spectrosc.* **195**, 236 (1999).
- [11] E. Kuznetsova, M. Gacesa, P. Pellegrini, S. F. Yelin, and R. Côté, *New J. Phys.* **11**, 055028 (2009).
- [12] B. C. Sawyer, B. K. Stuhl, M. Yeo, T. V. Tscherbul, M. T. Hummon, Y. Xia, J. Klos, D. Patterson, J. M. Doyle, and J. Ye, *Phys. Chem. Chem. Phys.* **13**, 19059 (2011).
- [13] G. Quémener and P. Julienne, *Chem. Rev.* **112**, 4949 (2012).
- [14] D. DeMille, *Phys. Rev. Lett.* **88**, 067901 (2002).
- [15] S. F. Yelin, K. Kirby, and R. Côté, *Phys. Rev. A* **74**, 050301 (2006).
- [16] E. Kuznetsova, R. Côté, K. Kirby, and S. F. Yelin, *Phys. Rev. A* **78**, 012313 (2008).
- [17] M. Mayle, G. Quémener, B. P. Ruzic, and J. L. Bohn, *Phys. Rev. A* **87**, 012709 (2013).
- [18] S. Chefdeville, T. Stoecklin, A. Bergeat, K. M. Hickson, C. Naulin, and M. Costes, *Phys. Rev. Lett.* **109**, 023201 (2012).
- [19] M. Lara, S. Chefdeville, K. M. Hickson, A. Bergeat, C. Naulin, J.-M. Launay, and M. Costes, *Phys. Rev. Lett.* **109**, 133201 (2012).
- [20] A. B. Henson, S. Gersten, Y. Shagam, J. Narevicius, and E. Narevicius, *Science* **338**, 234 (2012).
- [21] N. Geum, G.-H. Jeung, A. Derevianko, R. Côté, and A. Dalgarno, *J. Chem. Phys.* **115**, 5984 (2001).
- [22] E. P. Wigner, *Phys. Rev.* **73**, 1002 (1948).
- [23] H. R. Sadeghpour, J. L. Bohn, M. J. Cavagnero, B. D. Esry, I. I. Fabrikant, J. H. Macek, and A. R. P. Rau, *J. Phys. B* **33**, R93 (2000).
- [24] I. Simbotin, S. Ghosal, and R. Côté, *Phys. Rev. A*, **89**, 040701 (2014).
- [25] H. A. Bethe, *Phys. Rev.* **47**, 747 (1935).
- [26] U. Fano, *Phys. Rev.* **124**, 1866 (1961).
- [27] N. Balakrishnan, R. C. Forrey, and A. Dalgarno, *Phys. Rev. Lett.* **80**, 3224 (1998).
- [28] N. Balakrishnan, V. Kharchenko, R. C. Forrey, and A. Dalgarno, *Chem. Phys. Lett.* **280**, 5 (1997).
- [29] E. Garand, J. Zhou, D. E. Manolopoulos, M. H. Alexander, and D. M. Neumark, *Science* **319**, 72 (2008).
- [30] N. Balakrishnan, *J. Chem. Sci.* **124**, 311 (2012).
- [31] W. Bian and H.-J. Werner, *J. Chem. Phys.* **112**, 220 (2000).
- [32] N. Balakrishnan and A. Dalgarno, *Chem. Phys. Lett.* **341**, 652 (2001).
- [33] E. Bodo, F. A. Gianturco, N. Balakrishnan, and A. Dalgarno, *J. Phys. B* **37**, 3641 (2004).
- [34] K. Stark and H.-J. Werner, *J. Chem. Phys.* **104**, 6515 (1996).
- [35] M. T. Cvitas, P. Soldan, J. M. Hutson, P. Honvault, and J.-M. Launay, *J. Chem. Phys.* **127**, 074302 (2007).
- [36] D. Skouteris, J. F. Castillo, and D. E. Manolopoulos, *Comp. Phys. Comm.* **133**, 128 (2000).
- [37] I. Simbotin, S. Ghosal, and R. Côté, *Phys. Chem. Chem. Phys.* **13**, 19148 (2011).
- [38] I. Simbotin and R. Côté, *New J. Phys.*, in press (2015).
- [39] J. Wang, J. N. Byrd, I. Simbotin, and R. Côté, *Phys. Rev. Lett.* **113**, 025302 (2014).
- [40] J. R. Taylor, *Scattering Theory* (Dover Publications, Mineola, NY, 2006).
- [41] See page 523 in Ref. [42].
- [42] R. G. Newton, *Scattering Theory of waves and particles* (Dover Publications, Mineola, NY, 2002).
- [43] See page 343 in Ref. [42].
- [44] See page 335 in Ref. [42].
- [45] K. Willner and F. A. Gianturco, *Phys. Rev. A* **74**, 052715 (2006).
- [46] See page 528 in Ref. [42].
- [47] E. J. Heller and W. P. Reinhardt, *Phys. Rev. A* **5**, 757 (1972).
- [48] J. L. Nolte, B. H. Yang, P. C. Stancil, T.-G. Lee, N. Balakrishnan, R. C. Forrey, and A. Dalgarno, *Phys. Rev. A* **81**, 014701 (2010).
- [49] J. M. Hutson, M. Beyene, and M. L. González-Martínez, *Phys. Rev. Lett.* **103**, 163201 (2009).
- [50] J. M. Hutson, *New J. Phys.* **9**, 152 (2007).
- [51] A. Crubellier and E. Luc-Koenig, *J. Phys. B* **39**, 1417 (2006).
- [52] P. Pellegrini, M. Gacesa, and R. Côté, *Phys. Rev. Lett.* **101**, 053201 (2008).
- [53] M. Arndt, M. Ben Dahan, D. Guéry-Odelin, M. W. Reynolds, and J. Dalibard, *Phys. Rev. Lett.* **79**, 625 (1997).
- [54] J. Söding, D. Guéry-Odelin, P. Desbiolles, G. Ferrari, and J. Dalibard, *Phys. Rev. Lett.* **80**, 1869 (1998).